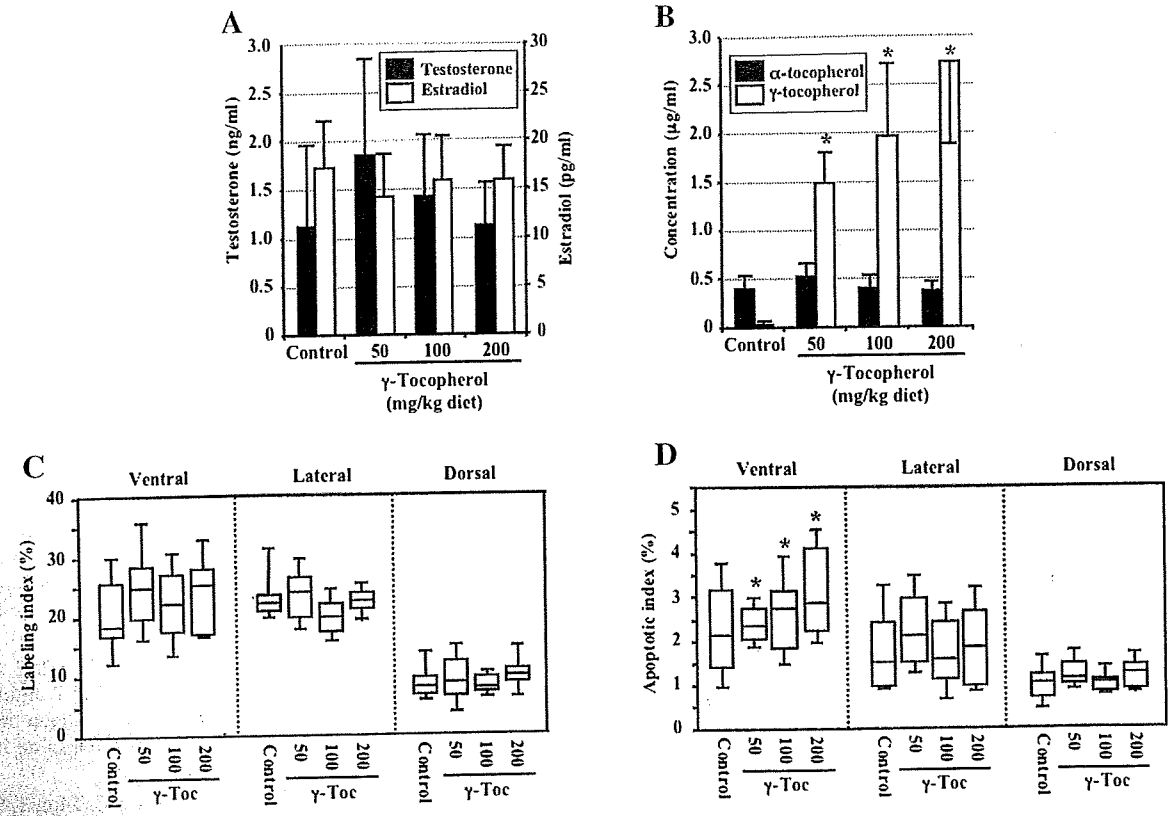

Fig. 3. Effects of γ-tocopherol on serum steroid hormones, plasma tocopherol levels, and labeling indices for Ki-67 and apoptotic cells (TUNEL) in individual prostatic lobes in Experiment 2. **A**: Serum levels of testosterone and estradiol. **B**: Plasma levels of tocopherols. Box plot data for (**C**) Ki-67 and (**D**) TUNEL indices in each prostate lobe of TRAP rats.

[31,32] but this controversial finding may be linked to particular biochemical activity and tissue distributions of the vitamin E isoform molecule. For instance, ingestion of α-tocopherol has been reported to result in reduction in the serum levels of γ-tocopherol [33–36]. In this context it should be noted that high serum concentrations of γ-tocopherols are associated with significantly lower risk of developing prostate cancer and protective effects of selenium and α-tocopherol were found only on the presence of high levels of γ-tocopherol [10].

In conclusion, the present investigation using the TRAP model provided clear evidence that γ-tocopherol can suppress prostate carcinogenesis with induction of apoptosis through caspase activation. In consideration of the lack of any toxic changes in organs such as the

TABLE IV. Quantitative Evaluation of Neoplastic Lesions in Prostates of TRAP Rats Treated With γ-Tocopherol (Experiment 2)

		Relative number of acini with histological characteristics (%)					
		Ventral lobe			Lateral lobe		
Treatment	No. of rats	LG-PIN	HG-PIN	ADC	LG-PIN	HG-PIN	ADC
Control	14	4.7 ± 1.6	92.3 ± 1.8	3.1 ± 0.8	19.1 ± 9.8	80.6 ± 9.7	0.4 ± 0.5
γ-Tocopherol 50 mg/kg	14	5.1 ± 2.4	93.1 ± 2.5	1.7 ± 1.4[a,c]	14.2 ± 6.0	85.5 ± 5.9	0.3 ± 0.3
γ-Tocopherol 100 mg/kg	14	4.8 ± 3.2	93.8 ± 2.9	1.4 ± 1.1[b,c]	12.5 ± 3.2	87.2 ± 3.1	0.2 ± 0.3
γ-Tocopherol 200 mg/kg	14	4.3 ± 1.9	94.2 ± 1.8	1.4 ± 0.8[b,c]	13.8 ± 5.9	86.0 ± 5.8	0.3 ± 0.3

LG-PIN, low grade prostatic intraepithelial neoplasia; HG, high grade; ADC, adenocarcinoma.
[a,b]$P < 0.05$ and 0.01 versus control, respectively.
[c]$P < 0.01$ versus control (Spearman's rank correlation coefficient test).

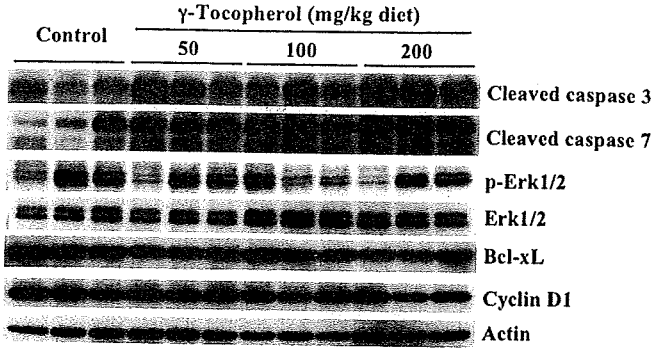

Fig. 4. Immunoblot analysis of caspases, MAPKs and other apoptosis-related proteins in ventral prostates of TRAP rats treated with γ-tocopherol in Experiment 2.

liver, kidneys, and heart, γ-tocopherol would appear to be a potential ideal agent for prostate cancer chemoprevention.

ACKNOWLEDGMENTS

This work was supported by a Grant-in-Aid for Cancer Research from the Ministry of Health, Labour and Welfare of Japan, a Grant-in-Aid for the 2nd Term Comprehensive 10-Year Strategy for Cancer Control from the Ministry of Health, Labour and Welfare of Japan and a grant from the Society for Promotion of Pathology of Nagoya, Japan.

REFERENCES

1. Parkin DM, Bray FI, Devesa SS. Cancer burden in the year 2000. The global picture. Eur J Cancer 2001;37:S4–S66.
2. Jemal A, Murray T, Ward E, Samuels A, Tiwari RC, Ghafoor A, Feuer EJ, Thun MJ. Cancer statistics, 2005. CA Cancer J Clin 2005; 55:10–30.
3. Franceschi S, La Vecchia C. Cancer epidemiology in the elderly. Crit Rev Oncol Hematol 2001;39:216–226.
4. Cunha GR, Donjacour AA, Cooks PS, Mee S, Bigsby RM, Higgins SJ, Sugimura Y. The endocrinology and developmental biology of the prostate. Endocr Rev 1987;8:338–362.
5. Denis LJ, Griffiths K. Endocrine treatment in prostate cancer. Semin Surg Oncol 2000;18:52–74.
6. Gronberg H. Prostate cancer epidemiology. Lancet 2003;361: 859–864.
7. Nelson WG, De Marzo AM, Isaacs WB. Prostate cancer. N Engl J Med 2003;349:366–381.
8. Shirai T, Asamoto M, Takahashi S, Imaida K. Diet and prostate cancer. Toxicology 2002;181–182:89–94.
9. Heinonen OP, Albanes D, Virtamo J, Taylor PR, Huttunen JK, Hartman AM, Haapakoski J, Malila N, Rautalahti M, Ripatti S, Maenpaa H, Teerenhovi L, Koss L, Virolainen M, Edwards BK. Prostate cancer and supplementation with α-tocopherol and β-carotene: Incidence and mortality in a controlled trial. J Natl Cancer Inst 1998;90:440–446.
10. Helzlsouer KJ, Huang H-Y, Alberg AJ, Hoffman S, Burke A, Norkus EP, Morris JS, Comstock GW. Association between α-tocopherol, γ-tocopherol, selenium, and subsequent prostate cancer. J Natl Cancer Inst 2000;92(24):2018–2023.
11. Huang H-Y, Alberg AJ, Norkus EP, Hoffman SC, Comstock GW, Helzlsouer KJ. Prospective study of antioxidant micronutrients in the blood and the risk of developing prostate cancer. Am J Epidemiol 2003;157:335–344.
12. Nomura AM, Stemmermann GN, Lee J, Craft NE. Serum micronutrients and prostate cancer in Japanese Americans in Hawaii. Cancer Epidemiol Biomarkers Prev 1997;6:487–491.
13. Weinstein SJ, Wright ME, Pietinen P, King I, Tan C, Taylor PR, Virtamo J, Albanes D. Serum α-tocopherol and γ-tocopherol in relation to prostate cancer risk in a prospective study. J Natl Cancer Inst 2005;97:396–399.
14. Asamoto M, Hokaiwado N, Cho YM, Takahashi S, Ikeda Y, Imaida K, Shirai T. Prostate carcinomas developing in transgenic rats with SV40 T antigen expression under probasin promoter control are strictly androgen dependent. Cancer Res 2001;61: 4693–4700.
15. Cho YM, Takahashi S, Asamoto M, Suzuki S, Inaguma S, Hokaiwado N, Shirai T. Age-dependent histopathological findings in the prostate of probasin/SV40 T antigen transgenic rats: Lack of influence of carcinogen or testosterone treatment. Cancer Sci 2003;94:153–157.
16. Said MM, Hokaiwado N, Tang M, Ogawa K, Suzuki S, Ghanem HM, Esmat AY, Asamoto M, Refaie FM, Shirai T. Inhibition of prostate carcinogenesis in probasin/SV40 T antigen transgenic rats by leuprorelin, a luteinizing hormone-releasing hormone agonist. Cancer Sci 2006;97:459–467.
17. Cho YM, Takahashi S, Asamoto M, Suzuki S, Tang T, Shirai T. Suppressive effects of antiandrogens, finasteride and flutamide on development of prostatic lesions in a transgenic rat model. Prostate Cancer Prost Dis 2007;10:378–383.
18. Seeni A, Takahashi S, Takeshita K, Tang M, Sugiura S, Sato SY, Shirai T. Suppression of prostate cancer growth by resveratrol in the transgenic rat for adenocarcinoma of prostate (TRAP) model. Asian Pac J Cancer Prev 2008;9:7–14.
19. Tang MX, Ogawa K, Asamoto M, Hokaiwado N, Seeni A, Suzuki S, Takahashi S, Tanaka T, Ichikawa K, Shirai T. Protective effects of citrus nobiletin and auraptene in transgenic rats developing adenocarcinoma of the prostate (TRAP) and human prostate carcinoma cells. Cancer Sci 2007;98:471–477.
20. Soeda S, Iwata K, Hosoda Y, Shimeno H. Daunorubicin attenuates tumor necrosis factor-α-induced biosynthesis of plasminogen activator inhibitor-1 in human umblical vein endothelial cells. Biochem Biophys Acta 2001;1538:234–241.
21. Galli F, Stabile AM, Betti M, Conte C, Pistilli A, Rende M, Floridi A, Azzi A. The effect of α- and γ-tocopherol and their carboxyethyl hydroxychroman metabolites on prostate cancer cell proliferation. Arch Biochem Biophys 2004;423(1):97–102.
22. Gysin R, Azzi A, Visarius T. γ-Tocopherol inhibits human cancer cell cycle progression and cell proliferation by down-regulation of cyclins. FASEB J 2002;16(14):1952–1954.
23. Jiang Q, Wong J, Fyrst H, Saba JD, Ames BN. γ-Tocopherol or combinations of vitamin E forms induce cell death in human prostate cancer cells by interrupting sphingolipid synthesis. Proc Natl Acad Sci USA 2004;101(51):17825–17830.
24. Yoshikawa S, Morinobu T, Hamamura K, Hirahara F, Iwamoto T. The effect of γ-tocopherol administration on α-tocopherol levels and metabolism in humans. Eur J Clin Nutr 2005;59:900–905.
25. Stone WL, Papas AM. Tocopherols and the etiology of colon cancer. J Natl Cancer Inst 1997;89:1006–1014.

26. Christen S, Woodall AA, Shigenaga MK, Southwell-Keely PT, Duncan MW, Ames BN. γ-Tocopherol traps mutagenic electrophiles such as NOx and complements α-tocopherol: Physiological implications. Proc Natl Acad Sci USA 1997;94:3217–3222.
27. Cooney RV, Franke AA, Harwood PJ, Hatch-Pigott V, Custer LJ, Mordan LJ. γ-Tocopherol detoxification of nitrogen dioxide: Superiority to α-tocopherol. Proc Natl Acad Sci USA 1997;90: 1771–1775.
28. Hensley K, Benaksas EJ, Bolli R, Comp P, Grammas P, Hamdheydari L, Mou S, Pye QN, Stoddard MF, Wallis G. New perspectives on vitamin E: γ-tocopherol and carboxyethylhydroxychroman metabolites in biology and medicine. Free Rad Biol Med 2004;36(1):1–15.
29. Jiang Q, Ames BN. γ-Tocopherol, but not α-tocopherol, decreases proinflammatory eicosanoids and inflammation damage in rats. FASEB J 2003;17(8):816–822.
30. Jiang Q, Elson-Schwab I, Courtemanche C, Ames BN. γ-Tocopherol and its major metabolite, in contrast to α-tocopherol, inhibit cyclooxygenase activity in macrophages and epithelial cells. Proc Natl Acad Sci USA 2000;97(21):11494–11499.
31. Investigators THaH-TT. Effects of long-term vitamin E supplementation on cardiovascular events and cancer. JAMA 2005; 293:1338–1347.
32. Lee I-M, Cook NR, Gaziano JM, Gordon D, Ridker PM, Manson JE, Hennekens CH, Buring JE. Vitamin E in the primary prevention of cardiovascular disease and cancer. JAMA 2005; 294:56–65.
33. Handelman GJ, Machlin LJ, Fitch K, Weiter JJ, Dratz EA. Oral α-tocopherol supplements decrease plasma γ-tocopherol levels in humans. J Nutr 1985;115:807–813.
34. Li D, Saldeen T, Romeo F, Mehta JL. Relative effects of α- and γ-tocopherol on low-density lipoprotein oxidation and superoxide dismutase and nitric oxide synthase activity and protein expression in rats. J Cardiovasc Pharmacol Ther 1999;4:219–226.
35. Mahabir S, Coit D, Liebes L, Brady MS, Lewis JJ, Roush G, Nestle M, Fry D, Berwick M. Randomized, placebo-controlled trial of dietary supplementation of α-tocopherol on mutagen sensitivity levels in melanoma patients: A pilot trial. Melanoma Res 2002; 12:83–90.
36. White E, Kristal AR, Shikany JM, Wilson AC, Chen C, Mares-Perlman JA, Masaki KH, Caan BJ. Correlates of serum α- and γ-tocopherol in the Women's Health Initiative. Ann Epidemiol 2001;11:136–144.

The Prostate 70:229–238 (2010)

Tranilast Suppresses Prostate Cancer Growth and Osteoclast Differentiation In Vivo and In Vitro

Shinya Sato,[1]* Satoru Takahashi,[1] Makoto Asamoto,[1] Taku Naiki,[1,2] Aya Naiki-Ito,[1] Kiyofumi Asai,[3] and Tomoyuki Shirai[1]

[1]Department of Experimental Pathology and Tumor Biology, Graduate School of Medical Sciences, Nagoya City University, Nagoya, Japan
[2]Department of Nephro-Urology, Graduate School of Medical Sciences, Nagoya City University, Nagoya, Japan
[3]Department of Molecular Neurology, Graduate School of Medical Sciences, Nagoya City University, Nagoya, Japan

BACKGROUND. In bone metastatic sites, prostate cancer cells proliferate on interacting with osteoclasts. Tranilast, which is used for an antiallergic drug, has been shown to inhibit growth of several cancers and stromal cells. The present study was conducted to assess suppressive effects of Tranilast on prostate cancer growth and osteoclast differentiation in vivo and in vitro.
METHODS. In vivo, rat prostate cancer tissue was transplanted onto cranial bones of F344 rats and Tranilast was given for 9 days at doses of 0, 200, or 400 mg/kg/day. In vitro, human prostate cancer cell lines, LNCaP, PC3, and DU145, the rat prostate cancer cell line, PLS-10, and rat bone marrow cells were similarly treated with the agent.
RESULTS. In vivo, tumor volumes were significantly decreased in the high dose group. While cell proliferation did not appear to be affected, apoptosis was induced and tumor necrosis was apparent. Cranial bone defects were decreased in the high dose group. In vitro, cell proliferation rates of all four cell lines were reduced by Tranilast and increased apoptosis was observed in LNCaP and PLS-10. In addition, Tranilast significantly reduced osteoclast differentiation of rat bone marrow cells. Western blot analysis of PLS-10 and LNCaP revealed that phospho-GSK3β was up-regulated and phospho-Akt was down-regulated.
CONCLUSIONS. Tranilast here suppressed rat prostate cancer growth and osteoclast differentiation. Growth of human prostate cancer cells was also inhibited. Thus, this agent deserves consideration as a candidate for conventional therapy of bone metastatic prostate cancer. *Prostate 70: 229–238, 2010.* © 2009 Wiley-Liss, Inc.

KEY WORDS: **Tranilast; bone microenvironment; prostate cancer; bone metastasis; osteoclast**

INTRODUCTION

Prostate cancer is the most common cancer among men in the United States [1], and is also becoming more frequent in Japan [2]. In advanced stages, patients frequently develop bone metastases and suffer from a variety of symptoms including bone pain, fractures, spinal cord compression, nerve root impingement, and bone marrow failure [3–5]. Therapeutic approaches such as radical prostatectomy and radiotherapy are curative for localized disease [6,7], but no curative treatments for bone metastatic prostate cancer are available. There is thus an urgent need for novel therapeutic approaches for the treatment of bone metastatic prostate cancer.

Generally, it is likely that cancer metastases depend on the interaction between tumor cells and stromal cells in the organ microenvironment [8,9]. In bone metastatic sites, prostate cancer cells interact with osteoclasts and osteoblasts, and proliferation is increased [10,11]. Consequently, inhibition of tumor cell growth as well

*Correspondence to: Shinya Sato, Department of Experimental Pathology and Tumor Biology, Graduate School of Medical Sciences, Nagoya City University, Nagoya 467-8601, Japan.
E-mail: satopin@med.nagoya-cu.ac.jp
Received 17 April 2009; Accepted 12 August 2009
DOI 10.1002/pros.21056
Published online 29 September 2009 in Wiley InterScience (www.interscience.wiley.com).

as osteoclast differentiation in the bone microenvironment can be considered important strategies for bone metastatic prostate cancer treatment.

Previously, we established transplantable rat prostate carcinomas from tumors that were originally induced by 3,2′-dimethyl-4-aminobiphenyl and testosterone propionate in F344 rats (PLS-P) [12,13]. Using PLS-P, we developed a syngenic rat model that shares characteristics with human prostate cancer bone metastasis regarding tumor–stromal interactions [14,15]. When PLS-P (androgen-independent, moderately differentiated adenocarcinoma) was transplanted onto the surface of rat calvaria, we observed osteolytic and osteoblastic changes at the tumor–bone interface, mimicking the histopathological features of bone metastases of human prostate cancer. Recently we used our animal model to provide evidence that osteoclasts contribute to growth of prostate cancer cells in the bone microenvironment by providing TGFβ from bone matrix [14,15], underlining its utility as a tool for examination of prostate carcinoma behavior in the bone microenvironment.

Tranilast, *N*-(3′4′-dimethoxycinnamonyl) anthranilic acid (*N*-5′), was developed in Japan as an antiallergic drug about 30 years ago [16]. Recently, it was found to inhibit proliferation of stromal cells such as fibroblasts, myofibroblasts and vascular smooth muscle cells in vitro and in vivo [17–21]. It also inhibits proliferation of desmoplastic tumors such as scirrhous gastric cancer and pancreatic cancer [22–24]. Furthermore tumor growth suppressive effects have been shown for various types of neoplasm [25–28].

Based upon the available findings, we hypothesized that Tranilast might suppress prostate cancer cell proliferation and osteoclast differentiation in the bone microenvironment. We therefore performed this in vitro/in vivo study using prostate cancer cell lines and rat bone marrow primary culture as well as our animal model.

MATERIALS AND METHODS

Animals

A total of 42 male rats of F344 were obtained at 5 weeks of age from Charles River Japan (Atsugi, Japan) for in vivo study, and three 4-week-old male rats were also obtained for rat bone marrow primary culture. All rats were maintained in plastic cages in an air-conditioned room at 22 ± 2°C and 55 ± 5% humidity. Food (Oriental MF; Oriental Yeast, Tokyo, Japan) and tap water were available ad libitum.

Tumor Tissue

PLS-P derived from carcinogen-induced rat prostate cancer was used in the present experiment as a transplantable prostate cancer. The details of the rat prostate cancer tissue are as previously reported [12–15].

Prostate Cancer Cell Lines

PC3, LNCaP, and DU145 were obtained from the American Type Culture Collection (ATCC). PLS-10, an androgen-independent rat prostate adenocarcinoma line established from PLS-P, was reported previously [29]. All four cell lines were maintained in RPMI 1640 media (Invitrogen, Carlsbad, CA) containing 10% FBS (Invitrogen) and 1% antibiotics (Antibiotic–Antimycotic, Invitrogen).

Animal Experiment

Approximately 0.3 g aliquots of PLS-P were transplanted onto cranial bones of 6-week-old male F344 rats under anesthesia. PLS-P was also transplanted subcutaneously into the flanks of F344 rats for evaluating the efficacy of Tranilast on prostate cancer in the subcutaneous microenvironment. For this, an incision of about 1 cm was made in the skin at the top of the head or the flank and a pocket beneath the skin was formed using forceps. The prostate tumor tissue was then inserted into the pocket, and the incision was closed using autoclips (BD Biosciences, Bedford, MA). Tumor sizes and body weights were measured every 3 days. One week after transplantation, autoclips were removed, and rats were divided into three groups (groups of rats with PLS-P transplanted onto the cranial bone; n = 8, groups of rats with PLS-P transplanted subcutaneously into the flank; n = 6). Tranilast (generously provided by KISSEI Pharmaceutical Co., Ltd, Nagano, Japan) was suspended in 0.5% methylcellulose solution (Wako, Osaka, Japan) and administered intragastrically at doses of 200 (low dose group) or 400 mg/kg/day (high dose group), once a day from day 9 to day 17 after tumor transplantation. In groups of rats with PLS-P transplanted subcutaneously into the flank, Tranilast was administered from day 9 to day 21 after transplantation. Rats in the control group received the methylcellulose vehicle alone. In groups of rats with PLS-P transplanted onto the cranial bone, at sacrificed on day 17, X-ray radiography of transplantation sites was performed with XED-125M (Shimazu, Tokyo, Japan), and cranial tumors with part of the calvarias were excised en bloc, fixed with 10% buffered formalin solution and processed for histological examination. For quantitative analysis of bone destruction, bone destruction length per total cranial bone length in hematoxylin and eosin (H&E) stained sections was examined under a light microscope connected to an image analysis system, the Image Processor for Analytical Pathology (IPAP, Sumika Technos Corp., Osaka, Japan), to provide a bone destruction index

(BDI). The research was conducted according to the Guidelines for the Care and Use of Laboratory Animals of Nagoya City University Medical School and the experimental protocol was approved by the Institutional Animal Care and Use Committee (H20-07).

Histochemistry and Immunohistochemistry

Specimens were sectioned (5 μm) and stained with H&E. To identify osteoclasts, tartrate-resistant acid phosphatase (TRAP) (Acid Phosphatase Leukocyte kit, Sigma-Aldrich, St. Louis, MO) was applied to paraffin sections. Multinuclear cells were stained by TRAP, and counted at the tumor–bone interface. To assess cell proliferation, sections were treated with Ki67 antibody (DAKO, Denmark) and sequentially with antirabbit secondary antibody and avidin–biotin complex (Vectastatin Elite ABC kit; Vector Laboratory, Burlingame, CA), then binding sites were visualized with diamino-benzidine. Sections were then counterstained with hematoxylin for microscopic examination. Proliferating cells were quantified counting Ki67-positive cells at a magnification of 400×. To identify apoptotic cells in the tumors, TdT-mediated dUTP-digoxigenin nick-end labeling (TUNEL) staining using a TUNEL assay kit (Takara, Shiga, Japan) was also performed on sections according to the manual. The apoptosis rate was calculated as the number of TUNEL positive tumor cells per total cell number at a magnification of 400× for three or four randomly selected areas. At least 1,000 cells were counted per lesion for the evaluation. TUNEL-positive cells and TUNEL-positive necrotic areas were assessed with the IPAP (Sumika Technos Corp.).

Rat Bone Marrow Primary Culture

Rat bone marrow cells were obtained from the tibiae of 4-week-old male rats as reported previously [15], seeded in 100-mm petri dishes (BD Biosciences, San Jose, CA) and cultured in α-MEM medium (Lonza, Switzerland) containing 10% FBS for 3 hr at 37°C. After incubation, the collected floating cells (osteoclast precursor cells) were cultured at 1.0×10^6 cells/ml/well in 24-well plates (Corning, Corning, NY) for 24 hr, then 10 ng/ml soluble RANKL (Wako), 0.1 ng/ml TGFβ (R&D Systems, Minneapolis, MN) and various concentrations of Tranilast (0, 0.001, 0.01, 0.1, and 1 mM) were added. The medium was refreshed after 3 days. After culturing for 1 week, cells were used for TRAP staining, and TRAP-positive multinucleated cells were counted.

Western Blot Analysis

PLS-10 and LNCaP treated with 1 mM Tranilast (most effective concentration for inhibiting cell proliferation and promoting apoptosis) for 1 hr were homogenized in RIPA buffer (150 mM NaCl, 50 mM Tris–HCl (pH 8.0), 1% NP-40, 0.5% sodium deoxycholate, 0.1% SDS, 1 mM phenylmethylsulphonyl fluoride, 1 mM sodium orthovanadate, and protease inhibitor cocktail (Roche, Mannheim, Germany)). Twenty micrograms aliquots of protein were resolved on SDS–PAGE and separated proteins were transferred to nitrocellulose membranes. The membranes were then incubated with the following antibodies: rabbit monoclonal antihuman and rat phospho-Akt (Thr308), phospho-Akt (Ser473), Akt, phospho-β-catenin (Ser33/37/Thr41), phosphor-β-catenin (Ser45), phospho-Bcl2, phospho-cMyc, phosphor-Erk5, phospho-FKHR, phospho-IκBα, phospho-JAK1, phosphor-NFκB, phospho-GSK3β (Ser9), GSK, phospho-p38MAPK, phospho-p42MAPK, phospho-PLCγ1, phospho-SAPK/JNK (these antibodies were purchased from Cell Signaling Technology, Lake Placid, NY), and β-actin (mouse monoclonal antibody, Sigma-Aldrich). Immunoreactions were demonstrated by the ECL-Plus detection system (GE Healthcare, Piscataway, NJ) after 1-hr incubation with secondary horseradish peroxidase-labeled antirabbit or antimouse antibodies (Cell Signaling Technology).

Cell Proliferation and Apoptosis Assays In Vitro

Cell proliferation of all 4 prostate cancer cell lines was assessed by WST-1 assay (Roche). Briefly, prostate cancer cells were plated in 96-well microplates at 1×10^4 cells/well in 100 μl of culture media and incubated for 24 hr with various concentrations of Tranilast (0, 0.001, 0.01, 0.1, and 1 mM) before exposure to 10 μl of WST-1 per the manufacturer's protocol. The formazan dye formed was quantified using a plate reader by the absorbance at 440 nm. Apoptosis of LNCaP and PLS-10 was assessed using a Guava Nexin kit and the Guava PCA system (Guava Technologies, Hayward, CA) utilizing two stains (annexin V and 7-amino actinomycin D [7-AAD]) to quantitate the percentage of apoptotic cells. The Nexin assay was performed according to the manufacturer's protocol with the following exception. Briefly, cells were incubated for 48 hr with various concentrations of Tranilast, and 1×10^6 cells/100 μl medium were then stained with annexin V and 7-AAD for 20 min on ice. Data were acquired on the Guava PCA system immediately.

RESULTS

Tumor Growth and Histological Analysis

Transplanted PLS-P grew to palpable size in 1 week after transplantation, adhering firmly to the calvaria in

all groups. Although the 0.3 g of transplanted tumor was palpable just after transplantation, the tumor was not palpable 2 or 3 days after transplantation. Then, after the transplanted tumor re-started growing, the tumor became palpable again about 1 week after transplantation. During the experimental period, mean body weights did not significantly differ among the groups, and no adverse signs such as diarrhea or weight loss were observed in Tranilast-treated groups. The tumor volume in the Tranilast high dose group was significantly decreased compared with that in the control group ($P = 0.018$, Fig. 1A). All palpable masses were histologically confirmed to be transplanted PLS-P tumors, and tumor cells invading the calvaria caused bone destruction (Fig. 1C). At the tumor–bone interface, extensive bone defects with many multinucleated cells and nodular osteoid formation with osteoblasts were observed (Fig. 1D). We also transplanted PLS-P subcutaneously into the flanks of F344 rats, and Tranilast was administered on the same schedule as the rats with cranial transplantation. The tumor volume in the Tranilast high dose group was also significantly decreased compared with that in the control group ($P = 0.033$, Fig. 1B).

Cell Proliferation and Apoptotic Rates for Prostate Tumors

Many Ki67-positive tumor cells were observed in tumors (Fig. 2A–C), but Ki67 positive cell indices did not reveal any differences in cell proliferation among the three groups (Fig. 2D). In the Tranilast high dose group, many TUNEL-positive cells were observed in the central region of the tumor (Fig. 3A). But in the control group, tumor cells had fewer TUNEL-positive cells (Fig. 3B). The percentage of TUNEL-positive cells and TUNEL-positive cell areas in tumors was significantly increased in the Tranilast high dose group ($P < 0.001$, Fig. 3C–F).

Degree of Bone Destruction by Prostate Tumor Invasion

Radiographs of cranial bone showed partial cranial bone defects at tumor transplanted sites (Fig. 4A). On histological analysis, the mean length of cranial bone defects in the Tranilast-high dose group was significantly decreased as compared to the control group ($P = 0.03$, Fig. 4B). Multinucleated cells in bone destruction sites were identified as osteoclasts by

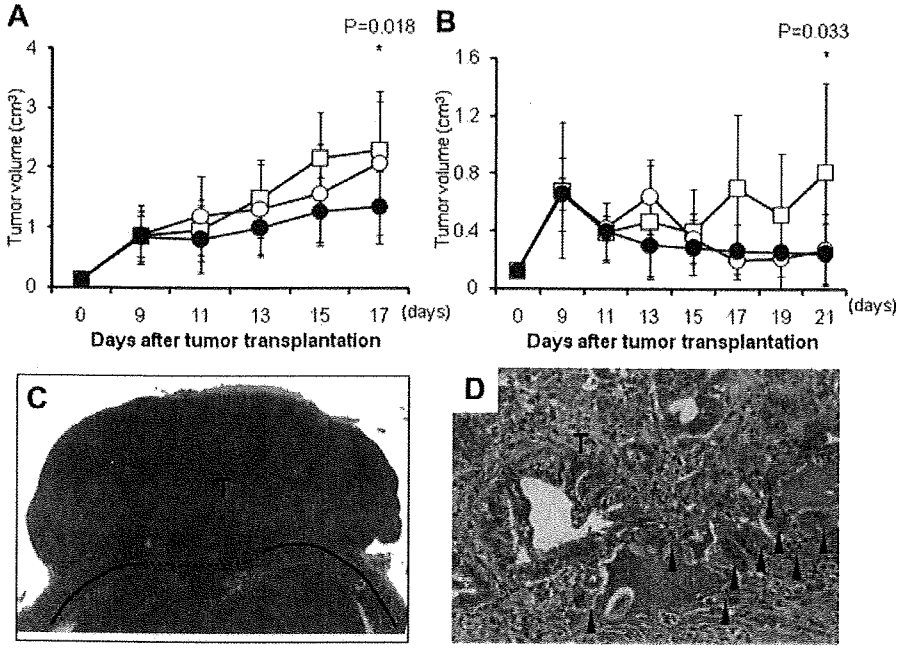

Fig. 1. Tumor growth and histological analysis of prostate cancer tissue on rat cranial bone. **A**,**B**: Sequential changes in cranial transplanted tumor volume (A) and subcutaneous transplanted tumor volume (B) (cm^3). Open squares, open circles, and closed circles represent the control group, Tranilast low dose group and Tranilast high dose group, respectively. Values are mean ± SD. **C**: Histological appearance of a tumor (T) invading and destroying rat cranial bone. The solid line indicates cranial bone and the dotted line indicates disrupted cranial bone. **D**: Higher magnification of the tumor–bone interface. Bone defects with multinucleated cells (arrowhead) are apparent with growth of a well-differentiated adenocarcinoma (T). C, 20× magnification. D, 200× magnification. [Color figure can be viewed in the online issue, which is available at www.interscience.wiley.com.]

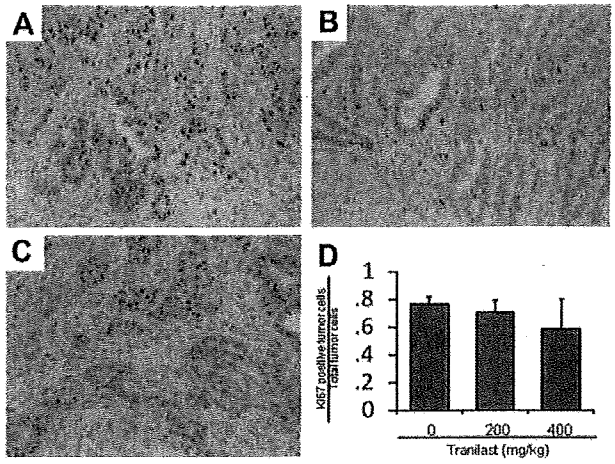

Fig. 2. Ki67 immunohistochemistry and labeling indices. **A–C**: Immunohistochemistry of Ki67 in the control group (A), Tranilast low dose group (B), and high dose group (C). Positive staining is evident in the nuclei of tumor cells. Ki67 positive cell labeling indices (mean ± SD values) are graphically presented in D. A–C: 200× magnification.

positive staining for TRAP (Fig. 4C). The numbers of multinucleated cells did not significantly differ among the three groups, but the multinucleated cell density per unit length (1 μm) of remaining cranial bone was marginally decreased in the Tranilast high dose group ($P = 0.078$, Fig. 4C).

Cell Proliferation and Apoptosis of Prostate Cancer Cells In Vitro

WST-1 assays revealed cell proliferation of all prostate cancer cell lines to be significantly decreased by Tranilast treatment at 0.1 and 1 mM ($P < 0.001$, Fig. 5A–D). The apoptotic cell ratios in the LNCaP and PLS-10 were increased in a Tranilast concentration-dependent manner (Fig. 5E).

Osteoclast Differentiation In Vitro

In the primary culture of rat bone marrow cells, the numbers of TRAP-positive multinucleated cells were significantly reduced by the high but not low dose of Tranilast (Fig. 6A–E).

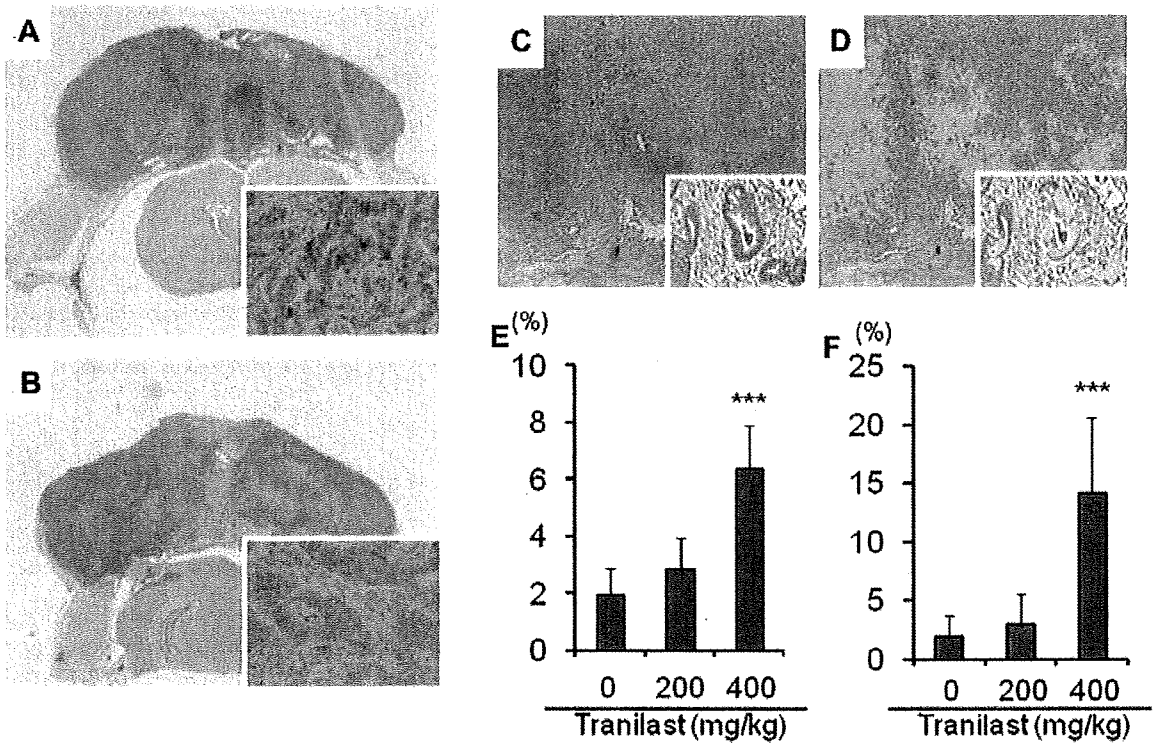

Fig. 3. TUNEL staining and labeling indices. **A,B**: TUNEL staining of tumor in Tranilast high-dose group (A) and the control group (B). Positive staining in the nuclei of tumor cells (inset). The TUNEL positive area (brown, **C**) was measured with an image analyzer (green, **D**). TUNEL positive cell labeling indices are presented in (**E**). **F**: The percentage TUNEL positive cell areas. Values are mean ± SD. ***$P < 0.001$ versus the control. A,B: 20× magnification. C,D: 100× magnification.

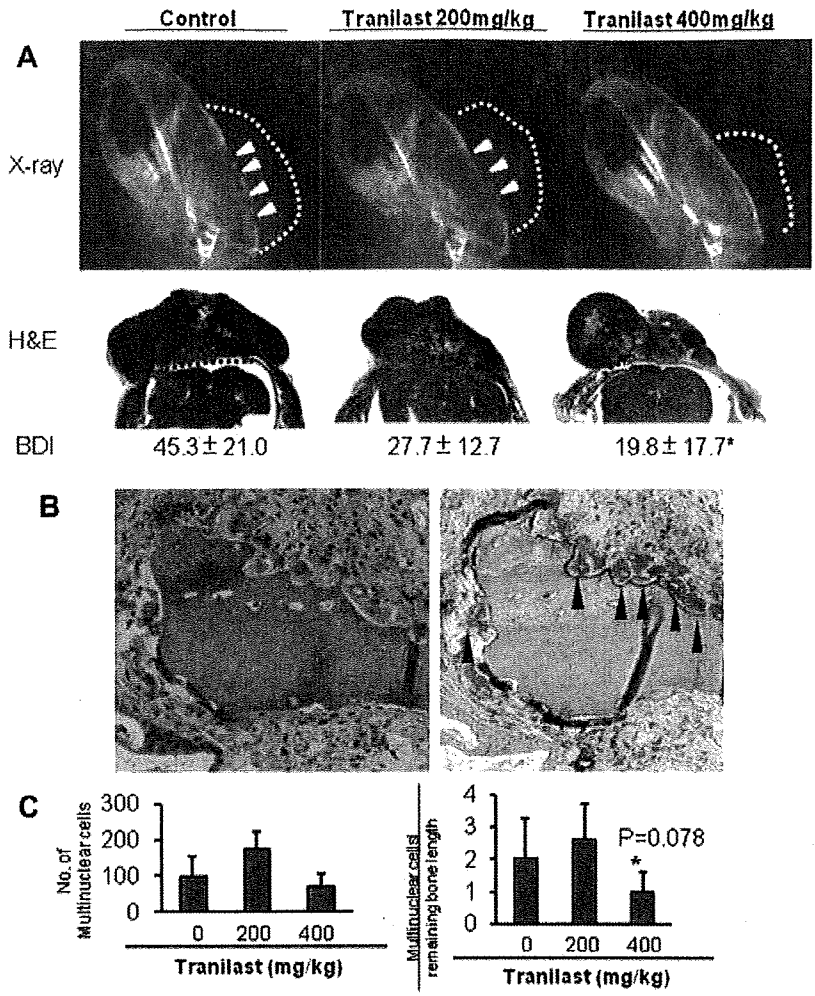

Fig. 4. Bone destruction and osteoclast induction in vivo. **A**: X-ray photographs and histological appearance of the tumor and rat cranial bone. In X-ray photographs, dotted lines indicate the tumor outline, and arrowheads indicate bone destruction. In the H&E stained section, the dotted line shows the area of bone destruction. BDI; destroyed bone length/total cranial bone length interacted with the tumor. **B**: Osteoclast induction in the tumor. Arrowheads indicateTRAP-positive multinucleated cells. **C**: The number of multinucleated cells (left graph) and the multinucleated cell density per unit length (l μm) of cranial bone (right graph). *$P < 0.078$ versus the control. Values are mean ± SD. A, 10× magnification. B, 200× magnification.

Western Blot Analysis

Initially, we analyzed expression of several phosphorylated proteins associated with cell proliferation or apoptosis by Western blot (Fig. 7A). From the results, we chose pAkt as the most down-regulated and pGSK3β as the most up-regulated protein by Tranilast treatment, and Western blot analysis was carried out to determine the time course of GSK3β phosphorylation. As shown in Figure 7B, GSK3β phosphorylation at 1, 2, 6, and 12 hr after Tranilast treatment was increased in PLS-10 cells compared with the control value. Conversely, Thr (308) Akt phosphorylation at 1 hr after Tranilast treatment was decreased (Fig. 7C). Similar results were obtained with LNCaP cells (data not shown).

DISCUSSION

The present study demonstrated that Tranilast significantly suppresses rat prostate tumor growth on the cranial bone. Tranilast increased TUNEL positive cells in vivo and promote apoptosis in rat and human prostate cancer cells in vitro. Thus, it is clear that Tranilast has a potential to suppress prostate cancer growth by inducing apoptosis.

We chose doses of Tranilast in the in vivo study that were equivalent to the maximum doses in clinical use

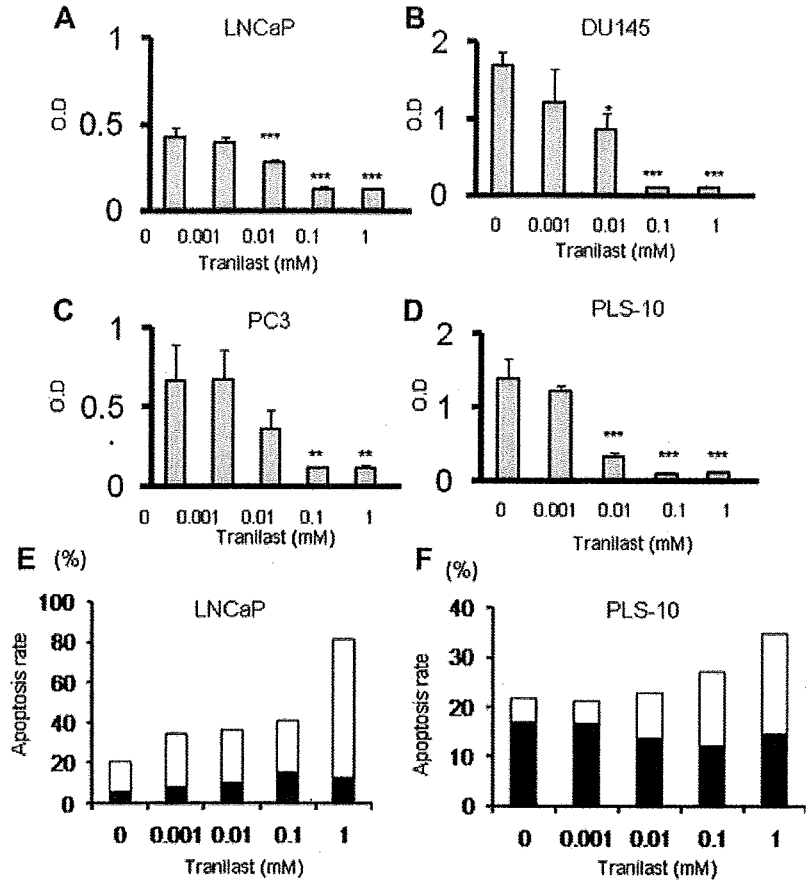

Fig. 5. Effects of Tranilast on cell proliferation and apoptosis of prostate cancer cell lines in vitro. WST-1 assay for analysis of cell proliferation in human (**A–C**, LNCaP, DU145, and PC3) and rat (**D**, PLS-10) prostate cancer cell lines. Data are mean ± SD values. **E,F**: The percentage of early cell apoptosis (white bar) and late cell apoptosis (black bar) of LNCaP (E) and PLS-10 (F). $^{**}P < 0.01$ versus the control. $^{***}P < 0.001$ versus the control.

[30] and chose concentrations of Tranilast in the in vitro study that were equivalent to the in vivo doses [31]. Although Tranilast dramatically suppressed the growth of cancer cells in vitro, it did not in the in vivo model. The reasons for this discrepancy are unknown but similar differences between in vivo and in vitro have also been found in other studies [32–37]. They mentioned this difference could be due to the three-dimensional nature of tumors in vivo as compared to the two-dimensional nature of monolayer cultures in vitro [32–34], and promotive effects of stromal cells on tumor cell proliferation in vivo [35–37]. In addition, we speculate that the inhibitory effect of Tranilast on prostate cancer cell proliferation in vivo was abrogated by the promoting effect of TGFβ on prostate cancer cell proliferation, which we have previously demonstrated [15].

As shown by Western blot analyses, Tranilast reduced Akt phosphorylation and induced GSK3β phosphorylation in rat and human prostate cancer cell lines. Akt phosphorylation is associated with promotion of proliferation of cancer cells including prostate cancer [38–40], and GSK3β phosphorylation is linked to inhibition of cell proliferation [41,42]. Thus, inhibitory effects of Tranilast on prostate cancer cell proliferation may be due to regulation of Akt and GSK3β phosphorylation.

Reduced bone destruction by Tranilast might further be considered at least partially due to growth inhibition of the tumors. Since osteoclast cell density per unit length of the bone was decreased by Tranilast, and osteoclast differentiation was clearly inhibited in vitro, the observed suppression of bone destruction might also be attributable to inhibition of osteoclast differentiation in the bone microenvironment.

Taken the results of the present study together, Tranilast may suppress prostate cancer growth and bone destruction by inducing tumor cell apoptosis and

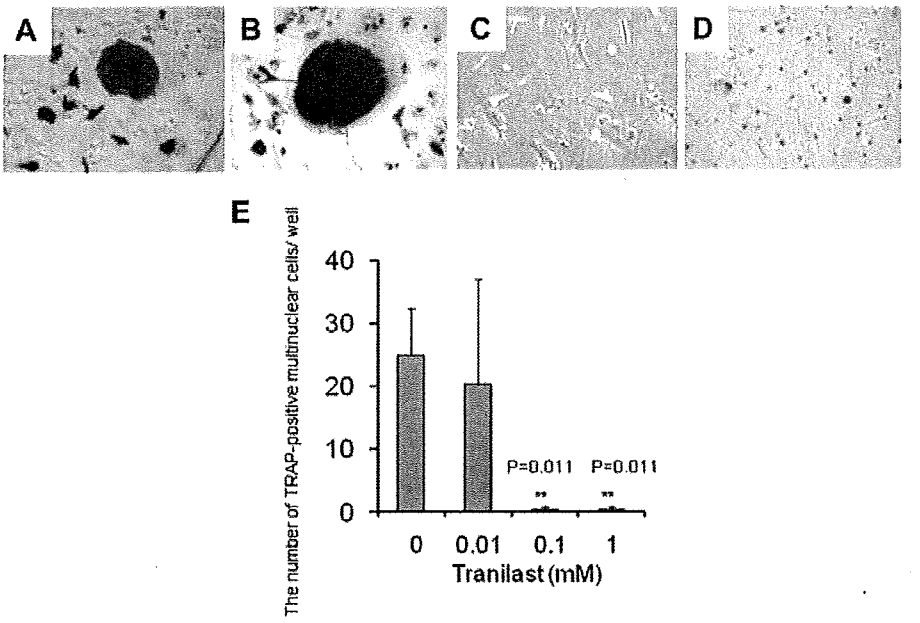

Fig. 6. Tranilast inhibits osteoclast differentiation. Rat bone marrow cells were cultured with control medium (**A**), Tranilast 0.01 mM (**B**), Tranilast 0.1 mM (**C**), and Tranilast 1 mM (**D**). The number of TRAP-positive multinucleated cells was significantly reduced by the high but not low dose (**E**). The averages of quadruplicate cultures for each group are graphically presented. Data are mean ± SD. A–E, 200× magnification. [Color figure can be viewed in the online issue, which is available at www.interscience.wiley.com.]

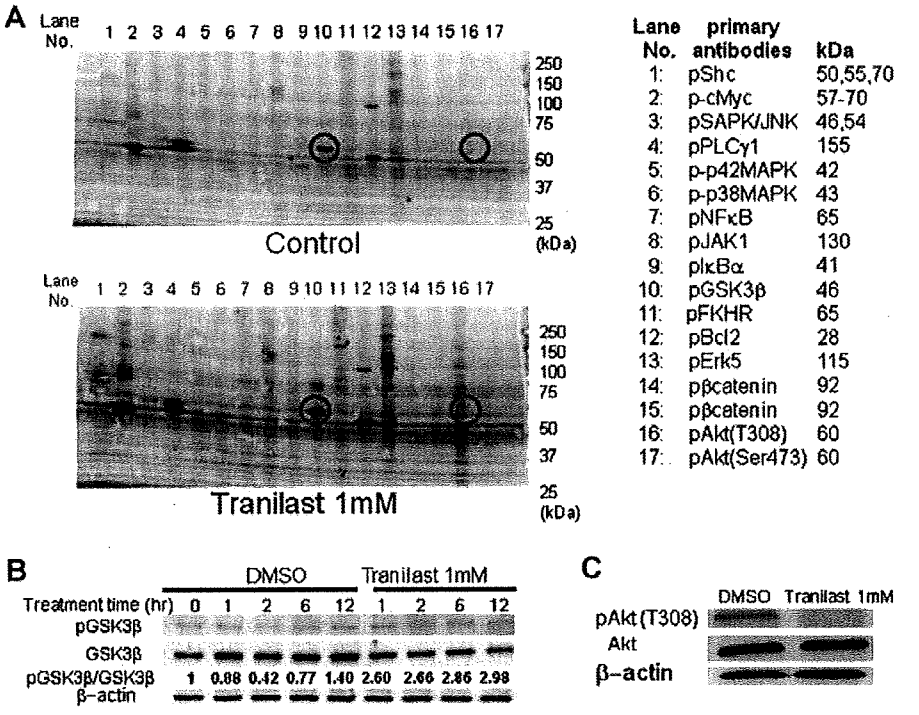

Fig. 7. Protein expression associated with cell proliferation and cell apoptosis in PLS-10. **A**: Western blot analysis of multiple proteins associated with cell proliferation and cell apoptosis. The lane numbers are for the primary antibodies on the right side. Significant spots were indicated with open squares. **B**: Chronological change of GSK3β phosphorylation on Western blotting. **C**: Expression of phosphorylated Akt on Western blotting. [Color figure can be viewed in the online issue, which is available at www.interscience.wiley.com.]

inhibiting osteoclast differentiation in the bone microenvironment.

CONCLUSIONS

Tranilast thus might provide additional therapeutic effects in combination with conventional drugs such as androgen antagonists, chemotherapeutic agents, and molecular target drugs. Further investigations are clearly warranted to explore Tranilast as a beneficial therapeutic option for prostate cancer patients with bone metastasis.

ACKNOWLEDGMENTS

We thank Junji Kuroda (KISSEI Pharmaceutical Co., Ltd, Nagano, Japan) for providing Tranilast. We would also like to thank Dr. Mitsuru Futakuchi, Department of Molecular Toxicology, Graduate School of Medical Sciences, for his excellent guidance and for his support in this project.

REFERENCES

1. Jemal A, Siegel R, Ward E, Hao Y, Xu J, Murray T, Thun MJ. Cancer statistics, 2008. CA Cancer J Clin 2008;58(2):71–96.
2. Qiu D, Katanoda K, Marugame T, Sobue T. A Joinpoint regression analysis of long-term trends in cancer mortality in Japan (1958–2004). Int J Cancer 2009;124(2):443–448.
3. Major PP, Cook RJ, Chen BL, Zheng M. Survival-adjusted multiple-event analysis for the evaluation of treatment effects of zoledronic Acid in patients with bone metastases from solid tumors. Support Cancer Ther 2005;2(4):234–240.
4. Coleman RE. Clinical features of metastatic bone disease and risk of skeletal morbidity. Clin Cancer Res 2006;12 (20 Pt 2):6243s–6249s.
5. Brescia FJ, Portenoy RK, Ryan M, Krasnoff L, Gray G. Pain, opioid use, and survival in hospitalized patients with advanced cancer. J Clin Oncol 1992;10(1):149–155.
6. Taplin ME, Xie W, Bubley GJ, Ernstoff MS, Walsh W, Morganstern DE, Regan MM. Docetaxel, estramustine, and 15-month androgen deprivation for men with prostate-specific antigen progression after definitive local therapy for prostate cancer. J Clin Oncol 2006;24(34):5408–5413.
7. Speight JL, Roach M III. Advances in the treatment of localized prostate cancer: The role of anatomic and functional imaging in men managed with radiotherapy. J Clin Oncol 2007;25(8):987–995.
8. Bogenrieder T, Herlyn M. Axis of evil: Molecular mechanisms of cancer metastasis. Oncogene 2003;22(42):6524–6536.
9. Tuma RS. Mechanisms of metastasis: Theories focus on microenvironment, host factors, genes. J Natl Cancer Inst 2008;100(24): 1752–1754.
10. Mundy GR. Mechanisms of bone metastasis. Cancer 1997; 80(Suppl 8):1546–1556.
11. Roodman GD. Mechanisms of bone metastasis. N Engl J Med 2004;350(16):1655–1664.
12. Shirai T, Tamano S, Kato T, Iwasaki S, Takahashi S, Ito N. Induction of invasive carcinomas in the accessory sex organs other than the ventral prostate of rats given 3,2′-dimethyl-4-aminobiphenyl and testosterone propionate. Cancer Res 1991; 51(4):1264–1269.
13. Kato KTS, Mori S, Futakuchi M, Cui L, Ito N, Shirai T. Establishment of transplantable rat prostate carcinomas from primary lesions induced by 3, 2′-dimethyl-4-aminobiphenyl and testosterone. J Toxicol Pathol 1998;11:27–32.
14. Lynch CC, Hikosaka A, Acuff HB, Martin MD, Kawai N, Singh RK, Vargo-Gogola TC, Begtrup JL, Peterson TE, Fingleton B, Shirai T, Matrisian LM, Futakuchi M. MMP-7 promotes prostate cancer-induced osteolysis via the solubilization of RANKL. Cancer Cell 2005;7(5):485–496.
15. Sato S, Futakuchi M, Ogawa K, Asamoto M, Nakao K, Asai K, Shirai T. Transforming growth factor beta derived from bone matrix promotes cell proliferation of prostate cancer and osteoclast activation-associated osteolysis in the bone microenvironment. Cancer Sci 2008;99(2):316–323.
16. Azuma H, Banno K, Yoshimura T. Pharmacological properties of N-(3′,4′-dimethoxycinnamoyl) anthranilic acid (N-5′), a new anti-atopic agent. Br J Pharmacol 1976;58(4):483–488.
17. Isaji M, Nakajoh M, Naito J. Selective inhibition of collagen accumulation by N-(3,4-dimethoxycinnamoyl)anthranilic acid (N-5′) in granulation tissue. Biochem Pharmacol 1987;36(4): 469–474.
18. Miyazawa K, Kikuchi S, Fukuyama J, Hamano S, Ujiie A. Inhibition of PDGF- and TGF-beta 1-induced collagen synthesis, migration and proliferation by tranilast in vascular smooth muscle cells from spontaneously hypertensive rats. Atherosclerosis 1995;118(2):213–221.
19. Isaji M, Miyata H, Ajisawa Y, Takehana Y, Yoshimura N. Tranilast inhibits the proliferation, chemotaxis and tube formation of human microvascular endothelial cells in vitro and angiogenesis in vivo. Br J Pharmacol 1997;122(6):1061–1066.
20. Isaji M, Aruga N, Naito J, Miyata H. Inhibition by tranilast of collagen accumulation in hypersensitive granulomatous inflammation in vivo and of morphological changes and functions of fibroblasts in vitro. Life Sci 1994;55(15):PL287–PL292.
21. Suzawa H, Kikuchi S, Arai N, Koda A. The mechanism involved in the inhibitory action of tranilast on collagen biosynthesis of keloid fibroblasts. Jpn J Pharmacol 1992;60(2):91–96.
22. Yashiro M, Chung YS, Sowa M. Tranilast (N-(3,4-dimethoxycinnamoyl) anthranilic acid) down-regulates the growth of scirrhous gastric cancer. Anticancer Res 1997;17(2A):895–900.
23. Murahashi K, Yashiro M, Inoue T, Nishimura S, Matsuoka T, Sawada T, Sowa M, Hirakawa-Ys Chung K. Tranilast and cisplatin as an experimental combination therapy for scirrhous gastric cancer. Int J Oncol 1998;13(6):1235–1240.
24. Hiroi M, Onda M, Uchida E, Aimoto T. Anti-tumor effect of N-[3,4-dimethoxycinnamoyl]-anthranilic acid (tranilast) on experimental pancreatic cancer. J Nippon Med Sch 2002;69(3): 224–234.
25. Nie L, Oishi Y, Doi I, Shibata H, Kojima I. Inhibition of proliferation of MCF-7 breast cancer cells by a blocker of Ca(2+)-permeable channel. Cell Calcium 1997;22(2):75–82.
26. Yatsunami J, Aoki S, Fukuno Y, Kikuchi Y, Kawashima M, Hayashi SI. Antiangiogenic and antitumor effects of tranilast on mouse lung carcinoma cells. Int J Oncol 2000;17(6):1151–1156.
27. Platten M, Wild-Bode C, Wick W, Leitlein J, Dichgans J, Weller M. N-[3,4-dimethoxycinnamoyl]-anthranilic acid (tranilast) inhibits transforming growth factor-beta release and reduces migration and invasiveness of human malignant glioma cells. Int J Cancer 2001;93(1):53–61.

28. Noguchi N, Kawashiri S, Tanaka A, Kato K, Nakaya H. Effects of fibroblast growth inhibitor on proliferation and metastasis of oral squamous cell carcinoma. Oral Oncol 2003;39(3):240–247.
29. Nakanishi H, Takeuchi S, Kato K, Shimizu S, Kobayashi K, Tatematsu M, Shirai T. Establishment and characterization of three androgen-independent, metastatic carcinoma cell lines from 3,2′-dimethyl-4-aminobiphenyl-induced prostatic tumors in F344 rats. Jpn J Cancer Res 1996;87(12):1218–1226.
30. Fukuyama J, Ichikawa K, Miyazawa K, Hamano S, Shibata N, Ujiie A. Tranilast suppresses intimal hyperplasia in the balloon injury model and cuff treatment model in rabbits. Jpn J Pharmacol 1996;70(4):321–327.
31. Kusama H, Kikuchi S, Tazawa S, Katsuno K, Baba Y, Zhai YL, Nikaido T, Fujii S. Tranilast inhibits the proliferation of human coronary smooth muscle cell through the activation of p21waf1. Atherosclerosis 1999;143(2):307–313.
32. Horning JL, Sahoo SK, Vijayaraghavalu S, Dimitrijevic S, Vasir JK, Jain TK, Panda AK, Labhasetwar V. 3-D tumor model for in vitro evaluation of anticancer drugs. Mol Pharm 2008;5(5):849–862.
33. Beningo KA, Dembo M, Wang YL. Responses of fibroblasts to anchorage of dorsal extracellular matrix receptors. Proc Natl Acad Sci USA 2004;101(52):18024–18029.
34. Lee GY, Kenny PA, Lee EH, Bissell MJ. Three-dimensional culture models of normal and malignant breast epithelial cells. Nat Methods 2007;4(4):359–365.
35. Ko SC, Chapple KS, Hawcroft G, Coletta PL, Markham AF, Hull MA. Paracrine cyclooxygenase-2-mediated signalling by macrophages promotes tumorigenic progression of intestinal epithelial cells. Oncogene 2002;21(47):7175–7186.
36. Ramasamy R, Fazekasova H, Lam EW, Soeiro I, Lombardi G, Dazzi F. Mesenchymal stem cells inhibit dendritic cell differentiation and function by preventing entry into the cell cycle. Transplantation 2007;83(1):71–76.
37. Lechner S, Muller-Ladner U, Neumann E, Spottl T, Schlottmann K, Ruschoff J, Scholmerich J, Kullmann F. Thioredoxin reductase 1 expression in colon cancer: Discrepancy between in vitro and in vivo findings. Lab Invest 2003;83(9):1321–1331.
38. Cicenas J. The potential role of Akt phosphorylation in human cancers. Int J Biol Markers 2008;23(1):1–9.
39. Wang Y, Kreisberg JI, Ghosh PM. Cross-talk between the androgen receptor and the phosphatidylinositol 3-kinase/Akt pathway in prostate cancer. Curr Cancer Drug Targets 2007;7(6):591–604.
40. Blanco-Aparicio C, Renner O, Leal JF, Carnero A. PTEN, more than the AKT pathway. Carcinogenesis 2007;28(7):1379–1386.
41. Vene R, Larghero P, Arena G, Sporn MB, Albini A, Tosetti F. Glycogen synthase kinase 3beta regulates cell death induced by synthetic triterpenoids. Cancer Res 2008;68(17):6987–6996.
42. Sharma M, Chuang WW, Sun Z. Phosphatidylinositol 3-kinase/Akt stimulates androgen pathway through GSK3beta inhibition and nuclear beta-catenin accumulation. J Biol Chem 2002;277(34):30935–30941.

Angiotensin II Induces Oxidative Stress in Prostate Cancer

Hiroji Uemura,[1] Hitoshi Ishiguro,[1] Yukari Ishiguro,[2] Kouji Hoshino,[1] Satoru Takahashi,[3] and Yoshinobu Kubota[1]

[1]Department of Urology and [2]Department of Biology and Function in the Head and Neck, Yokohama City University Graduate School of Medicine, Yokohama, Japan and [3]Department of Experimental Pathology and Tumor Biology, Nagoya City University Graduate School of Medical Sciences, Nagoya, Japan

Abstract

Angiotensin II has been shown to be a cytokine especially acting as a growth factor. A local renin-angiotensin system has been identified in the prostate gland, and the physiologic function of angiotensin II seems to be similar in prostate cancer, as we previously reported. In the present study, we explored the biological role of angiotensin II in oxidative stress of prostate cancer cells. Activated Akt was determined, and the expression of oxidative stress-related proteins (p47phox, manganese superoxide dismutase 2, glutathione peroxidase) was examined by Western blotting in LNCaP cells, which were stimulated with angiotensin II and/or an angiotensin II receptor type 1 blocker, candesartan. To examine DNA damage induced by angiotensin II, 8-hydroxy-2′-deoxyguanosine was determined, and Western blots were analyzed to detect checkpoint proteins including p53, Chk2, and cdc2. Immunocytochemical studies of inducible nitric oxide synthase and superoxide anion radical (O_2^-) were done in LNCaP cells stimulated with angiotensin II. The phosphorylation of Akt was induced by angiotensin II treatment and inhibited by candesartan, as well as by LY294002, an inhibitor of phosphoinositide 3-kinase. Oxidative stress-related proteins were up-regulated by angiotensin II and inhibited by pretreatment with candesartan or catalase. The level of 8-hydroxy-2′-deoxyguanosine was increased by angiotensin II and conversely decreased by candesartan. Immunocytochemical studies showed that angiotensin II enhanced an inflammatory marker, inducible nitric oxide synthase, and the production of O_2^- radical. The hypothesis that angiotensin II has the potential to induce oxidative stress, which may be implicated in carcinogenesis of the prostate gland through long-term exposure to chronic inflammation is proposed. (Mol Cancer Res 2008;6(2):250–8)

Introduction

Prostate cancer is a major public health problem in men and the second leading cause of cancer death in the United States and Western developed countries (1). Recently, the prevalence of prostate cancer has also been increasing in Japan. Although the etiology has not been clarified, a possible cause is considered to be the westernization of the diet and life-style in Japan. At present, prostate cancer is thought to have a multifactorial etiology, with both environmental and genetic factors. We previously reported some genetic changes in prostate cancer cells and tissue detected using differential display method or GeneChip analysis. For example, the *liplin-α2* and *nmt55* genes have been identified using differential display method. The *liplin-α2* gene was down-regulated by dihydrotestosterone in prostate cancer cells, and the *nmt55* gene was up-regulated in prostate cancer tissue (2, 3). Also, we found that *neuroserpin* (*protease inhibitor 12*) expression was higher in prostate cancer than in normal prostate tissue by GeneChip analysis (4). Although numerous investigators have examined and identified genes related to prostate cancer, the mechanisms of prostate cancer development and progression remain obscure.

Because Virchow discovered leukocytes in neoplastic tissues and made the first connection between inflammation and cancer, the association of chronic inflammation with the development of cancer has been well recognized (5, 6). Under chronic inflammation, the release of reactive oxygen species (ROS) and reactive nitrogen species influences DNA damage in proliferating epithelium, leading to permanent genomic alterations, such as point mutations, deletions, or rearrangements (7). Oxidative or nitrosative stress occurs when excessive ROS and/or reactive nitrogen species are produced, overcoming cellular antioxidant defenses. Recently, a large number of investigations have consolidated the evidence that oxidative stress is implicated in carcinogenesis of the prostate gland. There have been accumulated reports indicating a reduction of antioxidant defense (8-10), elevated levels of ROS-related and reactive nitrogen species–related enzymes (11, 12), and

Received 6/20/07; revised 9/27/07; accepted 10/4/07.
Grant support: 2007 Strategic Research Project K19028 of Yokohama City University, grant-in-aid for Scientific Research from Ministry of Education, Culture, Science, and Technology, and COE research grant from Japan Society for the Promotion of Science.
The costs of publication of this article were defrayed in part by the payment of page charges. This article must therefore be hereby marked *advertisement* in accordance with 18 U.S.C. Section 1734 solely to indicate this fact.
Requests for reprints: Hiroji Uemura, Department of Urology, Yokohama City University School of Medicine, 3-9 Fukuura, Kanazawa-ku, Yokohama 236-0004, Japan. Phone: 81-45-787-2679; Fax: 81-45-786-5775. E-mail: hu0428@med.yokohama-cu.ac.jp

doi:10.1158/1541-7786.MCR-07-0289

increased levels of hydrogen peroxide (11) in prostatic intraepithelial neoplasia (PIN) and cancer. Nevertheless, the cause of oxidative stress linked to prostatic carcinogenesis has not been clarified.

Angiotensin II, which is a major effector peptide of the renin-angiotensin system (RAS), is well known to be an important factor in hypertension. The classic RAS has been identified in the kidney, heart, and vessel walls and characterized in terms of blood pressure and electrolyte/fluid homeostasis. On the other hand, involvement of a local RAS, with autocrine/paracrine roles rather than endocrine roles, has recently been documented in relation to growth/differentiation in specific organs. Interestingly, these phenomena also seem to occur in several cancer cells in which a local RAS is involved in the progression of cancer (13, 14). Recently, we have reported that angiotensin II affects the signal pathways in prostate cancer cells. Angiotensin II activates the signal transduction of mitogen-activated protein kinase and signal transducers and activators of transcription 3 and angiogenesis in prostate cancer cells (15). Also, angiotensin II facilitates the secretion of some growth factors and cytokines from prostate stromal cells, resulting in cell proliferation of prostate cancer (16). Of interest, many investigators have clarified that angiotensin II induces oxidative stress in vascular cells. Angiotensin II stimulates the production of ROS in endothelial cells by up-regulating the subunits of $NAD^+/NADP^+$ (NADPH) oxidases (17, 18).

Apart from the attention RAS has attracted in relation to its roles in the circulation, another function of local RAS related to cell proliferation and angiogenesis has recently been focused on, especially in carcinogenesis. To confirm the postulate that angiotensin II would induce ROS in prostate cancer cells, we examined the expression of oxidative stress-related proteins and DNA damage induced by angiotensin II and/or an angiotensin II receptor type 1 blocker (ARB). Our results support the hypothesis that angiotensin II generated in the prostate gland may be a cause of oxidative stress linked to prostatic carcinogenesis.

Results

Time Courses of Akt Phosphorylation

In the male reproductive system, the angiotensin II concentration in semen is higher than that in blood (19), which is important for enhancement of sperm motility and perforation of the oocyte. Earlier investigation of semen extender showed that 10 μmol/L angiotensin II increased retention of spermatozoa (20), and another report indicated that 100 nmol/L angiotensin II stimulated the acrosome reaction in spermatozoa (19). Therefore, 10 μmol/L angiotensin II may not be a high level in a physiologic condition. As we previously reported, 10 μmol/L angiotensin II stimulated the cell growth of prostate cancer cells in LNCaP and DU145 cells (14). Akt has been implicated in the regulation of a variety of signal transduction pathways, including those involved in cell proliferation (9, 21-23). To confirm the activation of Akt in LNCaP cells treated with angiotensin II, we did a time-course Western blot analysis. As shown in Fig. 1, phosphorylated Akt was time-dependently enhanced by 10 μmol/L angiotensin II treatment. Activation of Akt was shown from 1 h after the start of angiotensin II stimulation and gradually increased until 24 h. This phenomenon is different from the patterns of phosphorylations of mitogen-activated protein kinase and signal transducers and activators of transcription 3 shown in our previous report (14).

We then did Western blot to confirm the inhibition of Akt phosphorylation induced by angiotensin II. Figure 2A shows that Akt phosphorylation was induced in a dose-dependent manner by angiotensin II treatment at 1 and 10 μmol/L for 3 h. The Akt phosphorylation induced by 10 μmol/L angiotensin II was inhibited by pretreatment with 1 and 10 μmol/L candesartan, an ARB, for 30 min (Fig. 2B). Also, the Akt phosphorylation induced by 10 μmol/L angiotensin II was completely inhibited by pretreatment with 40 μmol/L LY294002, an inhibitor of phosphoinositide 3-kinase for 30 min (Fig. 2C). Also, pretreatment with 1,000 units/mL catalase, an antioxidant enzyme, for 30 min inhibited the Akt phosphorylation induced by 10 μmol/L angiotensin II for 3 h in LNCaP cells (Fig. 2D).

Expression of AT1 Receptor in LNCaP Cells

To confirm expression of the angiotensin II receptor type-1 receptor AT1 receptor, LNCaP cells were treated with 10 μmol/L angiotensin II for 24 h. As shown in Fig. 3, expression of the AT1 receptor was enhanced by angiotensin II treatment. Unlike Akt phosphorylation shown in Fig. 2, expression of the AT1 receptor was not inhibited by pretreatment with 10 μmol/L candesartan (CV11974) or 1,000 units/mL catalase for 30 min. Therefore, this result indicates that candesartan and catalase do not influence the expression of the AT1 receptor in LNCaP cells.

Expression of Oxidative Stress-Related Proteins Induced by Angiotensin II and ARB Treatment

We then did Western blot to examine whether oxidative stress-related proteins were affected when prostate cancer cells (LNCaP) were stimulated by angiotensin II treatment. Besides the major generation of ROS by mitochondrial respiration, superoxide is also generated by a family of enzymes known as NADPH oxidases, and p47phox is a crucial cytosolic regulatory subunit of NADPH oxidases. The expression of p47phox protein was enhanced by 10 μmol/L angiotensin II treatment for 24 h, as shown in Fig. 4 (*top*). As anticipated, this augmentation of p47phox expression was inhibited by pretreatment with 10 μmol/L candesartan or 1,000 units/mL catalase for 30 min.

To defend cells against oxidative stress, cells have multiple antioxidant enzymes. Mitochondrial superoxide dismutase 2

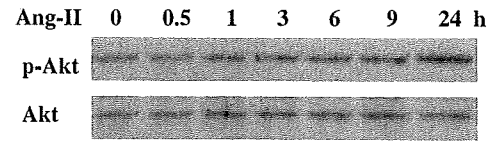

FIGURE 1. Western blots of phosphorylated Akt, total Akt, and actin. LNCaP cells cultured in steroid-free medium were harvested at the indicated times after angiotensin II (*Ang-II*; 10 μmol/L) treatment. The cells were lysed, and detergent extracts were immunoblotted with each antibody. Total protein (20 μg) was run and transferred to Immobilon-P transfer membrane and probed with phophorylated Akt and total Akt antibody.

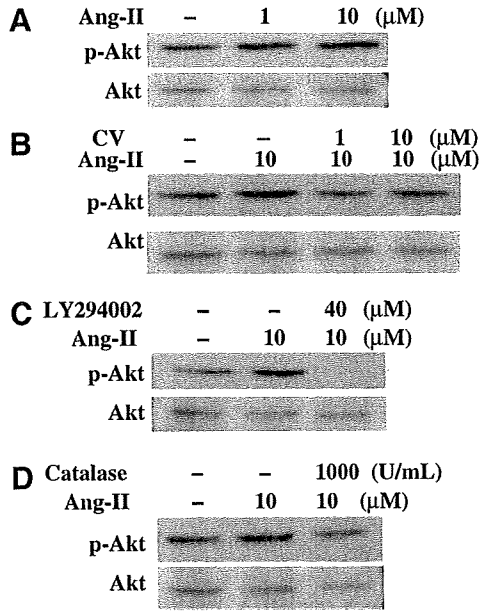

FIGURE 2. Phosphorylation of Akt induced by angiotensin II treatment and diminished by candesartan, LY294002, and catalase. **A.** LNCaP cells were stimulated with 1 or 10 μmol/L angiotensin II for 3 h. **B.** Cells were pretreated with 1 or 10 μmol/L candesartan (*CV*) for 30 min and harvested after 3 h of 10 μmol/L angiotensin II exposure. **C.** Cells were pretreated with 40 μmol/L LY294002, an inhibitor of phosphoinositide 3-kinase, for 30 min and harvested after 3 h of 10 μmol/L angiotensin II exposure. **D.** Cells were pretreated with 1,000 units/mL catalase, an antioxidant enzyme, for 30 min and harvested after 3 h of 10 μmol/L angiotensin II exposure. All Western blots of protein lysates were probed with antibodies to phosphorylated Akt (*p-Akt*) and total Akt.

(SOD2) is one of the first lines of defense. Because accumulated H_2O_2 leads to the production of hydroxyl radicals, cells are equipped with multiple enzymatic pathways for their removal. Glutathione peroxidase is one of three major pathways in the second line of defense against oxidative stress. We examined the expression of antioxidant enzymes SOD2 and glutathione peroxidase in LNCaP cells treated with 10 μmol/L angiotensin II for 24 h. As a result, the patterns of their protein expression were similar to that of p47phox expression. In brief, the expression of both antioxidant enzymes was enhanced by angiotensin II treatment for 24 h, and pretreatment with candesartan or catalase inhibited their expressions. The results of inhibition of both antioxidant enzymes by pretreatment with candesartan or catalase are convincing, because the pretreatment reduced superoxide generation associated with inhibition of p47phox.

Superoxide Anion (O_2^-) Induction by Angiotensin II Treatment

We determined the generation of the O_2^- radical, another important member of the ROS family, using fluorescent dye staining. Dihydroethidium (HE), which is a specific fluorescent dye for O_2^-, exhibits a red color after reaction with O_2^-.

After treatment with candesartan, catalase, or LY294002 for 30 min, LNCaP cells were treated with 10 μmol/L angiotensin II for 5 h. As shown in Fig. 5, angiotensin II enhanced the formation of the O_2^- radical (Fig. 5B) compared with control (Fig. 5A), whereas candesartan decreased O_2^- radical formation inside cells (Fig. 5C). Also, catalase decreased formation of the O_2^- radical induced by angiotensin II (Fig. 5D), because catalase is an antioxidant enzyme. Figure 5E shows that LY294002, an inhibitor of phosphoinositide 3-kinase, decreased the formation of the O_2^- radical induced by angiotensin II. We did semiquantitative digital image analysis of the O_2^- radical formation. Figure 5F indicates that angiotensin II enhanced the formation of the O_2^- radical ~28-fold higher than control and candesartan, catalase, and LY294002 decreased it, with which relative ratios compared with control were 0.6, 2.7, and 1.9, respectively.

To confirm whether angiotensin II enhances the formation of the O_2^- radical in prostate cancer cells, polyethylene glycol (PEG)–SOD, which is a representative antioxidant enzyme, was used as a positive control to show superoxide was being produced. Figure 6 shows that PEG-SOD clearly decreased formation of the O_2^- radical induced by angiotensin II (Fig. 6C). Semiquantitative image analysis indicates that PEG-SOD decreased O_2^- radical formation enhanced by angiotensin II at 14.2-fold down to 1.6-fold compared with control (Fig. 6D). These results provide direct evidence that angiotensin II can induce the generation of ROS in LNCaP cells and candesartan, as well as antioxidant enzymes, and an inhibitor of phosphoinositide 3-kinase can inhibit it.

Expression of Checkpoints Proteins and Measurement of 8-Hydroxy-2′-Deoxyguanosine Level

To confirm whether angiotensin II can provoke DNA damage in LNCaP cells, Western blot analyses to detect checkpoints proteins of DNA damage were done. After treatment with candesartan, catalase, or LY294002 for 30 min, LNCaP cells were treated with 10 μmol/L angiotensin II for 24 h. Figure 7A shows that angiotensin II induced the phosphorylation of p53 (Ser^{15}), Chk2 (Thr^{68}), and cdc2 (Tyr^{15}), and candesartan or catalase inhibited them. 4-Hydroxynonenal, a product of cell membrane lipid peroxidation, has been suggested to be a key mediator of oxidative stress–induced cell death (24, 25). Like the phosphorylation of checkpoint proteins, modification of proteins with 4-hydroxynonenal was enhanced by angiotensin II treatment and inhibited by candesartan or catalase (Fig. 7A). We also investigated whether androgen (dihydrotestosterone) influenced oxidative stress in LNCaP cells, which resulted in the induction of 4-hydroxynonenal by dihydrotestosterone in a dose-dependent manner (data not shown).

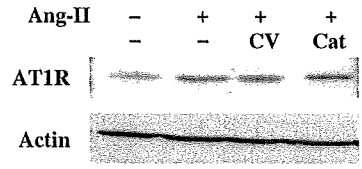

FIGURE 3. AT1 receptor expression induced by angiotensin II with/without candesartan and catalase. Western blots of AT1 receptor and actin. LNCaP cells were pretreated with 10 μmol/L candesartan or 1,000 units/mL catalase for 30 min and harvested after 24 h of 10 μmol/L angiotensin II exposure. Western blots of protein lysates were probed with anti-AT1 receptor and anti-actin antibodies.

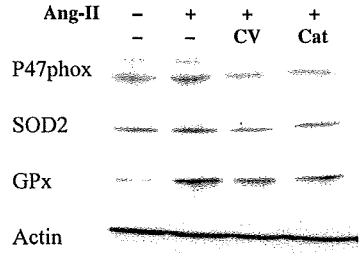

FIGURE 4. Expression of oxidative stress-related proteins induced by angiotensin II with/without candesartan and catalase. LNCaP cells were pretreated with 10 μmol/L candesartan or 1,000 units/mL catalase for 30 min and harvested after 24 h of 10 μmol/L angiotensin II exposure. Western blots of protein lysates (20 μg) were probed with antibodies to p47phox, glutathione peroxidase (*GPx*), SOD2, and actin.

As an indicator of DNA damage induced by oxidative stress, 8-hydroxy-2′-deoxyguanosine (8-OHdG) is routinely used. We examined the 8-OHdG level in the media of LNCaP cells treated with angiotensin II and/or candesartan (CV11974). The formation of 8-OHdG in LNCaP cells was significantly increased by treatment with 10 μmol/L angiotensin II (Fig. 7B) and significantly suppressed by 1 or 10 μmol/L CV11974 treatment ($P < 0.02$). These results were consistent with those of Western blots, which showed the pattern of checkpoint proteins and 4-hydroxynonenal expression induced by angiotensin II or candesartan treatment.

Inducible Nitric Oxide Synthase Expression in Prostate Cancer Cells with Angiotensin II and ARB Treatment

To confirm whether angiotensin II induces inflammation in prostate cancer cells, we did immunocytochemical staining of an enzyme dominantly expressed during inflammatory reactions. Inducible nitric oxide synthase (iNOS) is expressed in a variety of acute or chronic inflammatory human diseases, as well as in various types of cancer, including prostate cancer (26). iNOS antibody was used to detect the expression in LNCaP cells. The secondary antibody for iNOS was Cy3, labeled and raised against rabbit IgG. LNCaP cells were stimulated with 10 μmol/L angiotensin II after treatment with two different ARBs, candesartan and telmisartan (Tel), for 30 min. After 8 h stimulation, staining of iNOS and secondary antibodies was done. Figure 8 shows that intracellular expression of iNOS was induced by stimulation with angiotensin II (Fig. 8B) compared with the control (Fig. 8A), whereas candesartan and telmisartan diminished

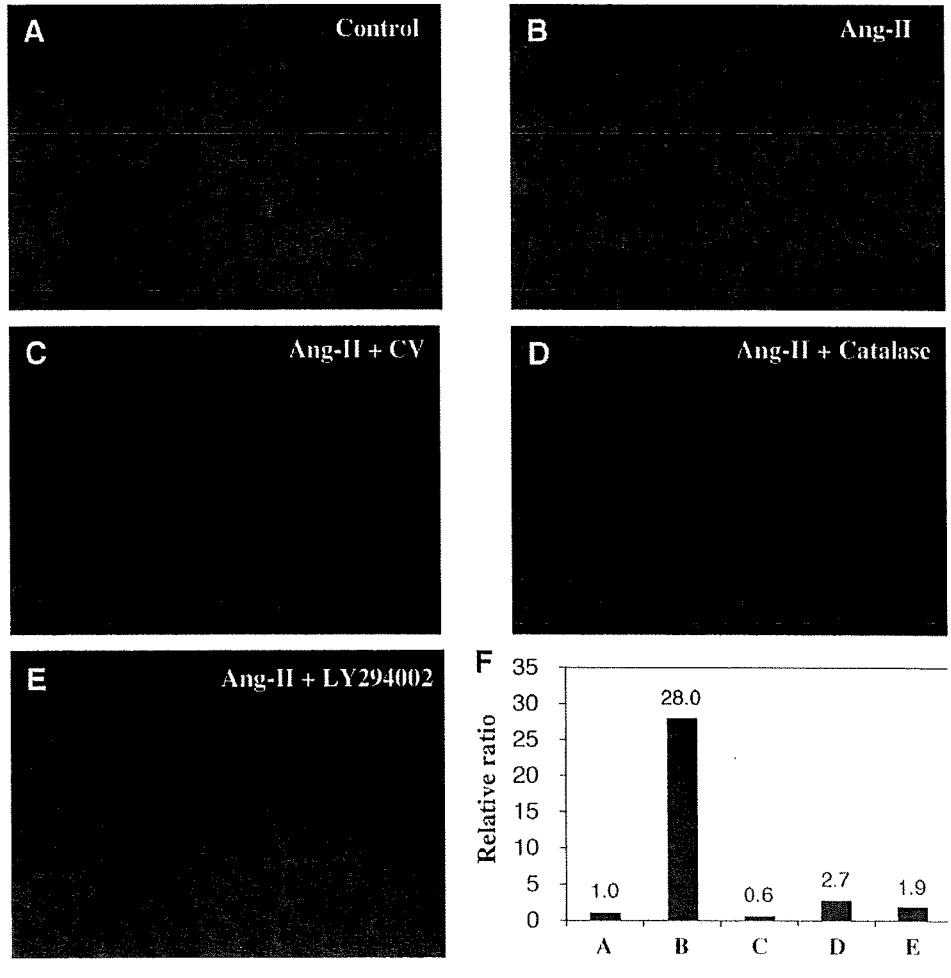

FIGURE 5. Determination of O_2^- production by H&E staining using confocal fluorescence microscope. Cells were plated onto a glass slip in a two-well plate for 24 h, followed by pretreatment with candesartan (10 μmol/L), catalase (1,000 units/mL), or LY294002 (40 μmol/L). Cells were then treated with angiotensin II (10 μmol/L) for 5 h. H&E was applied to the cells 30 min before treatment was completed. After being stained, the cells were washed twice with PBS and fixed with 10% buffered formalin. The images were captured with a confocal fluorescence microscope. **A.** Control. **B.** Angiotensin II. **C.** Angiotensin II and candesartan. **D.** Angiotensin II and catalase. **E.** Angiotensin II and LY294002. **F.** Semiquantitative digital image analysis of O_2^- production by H&E staining in each panel.

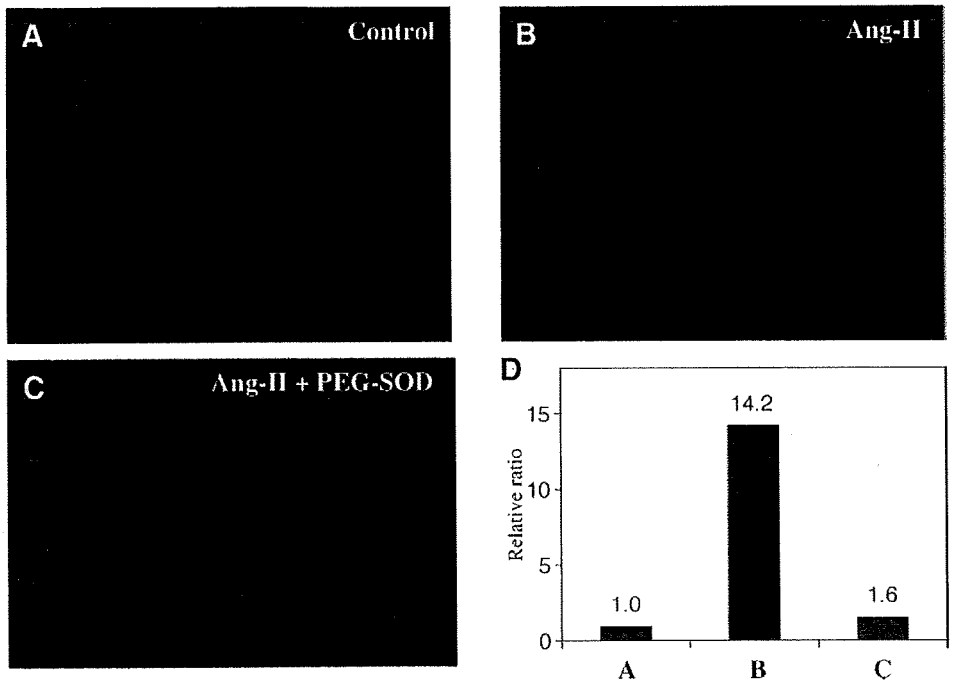

FIGURE 6. Determination of O_2^- production by H&E staining using confocal fluorescence microscope. Cells were plated onto a glass slip in a two-well plate for 24 h, followed by pretreatment with PEG-SOD (100 units/mL). Cells were then treated with angiotensin II (10 μmol/L) for 5 h. H&E was applied to the cells 30 min before treatment was completed. After being stained, the cells were washed twice with PBS and fixed with 10% buffered formalin. The images were captured with a confocal fluorescence microscope. **A.** Control. **B.** Angiotensin II. **C.** Angiotensin II and PEG-SOD. **D.** Semiquantitative digital image analysis of O_2^- production by H&E staining in each panel.

iNOS expression induced by angiotensin II (Fig. 8C and D). Like in LNCaP cells, similar phenomena were shown in DU145 cells (data not shown).

Discussion

Although angiotensin II is well known to be an important factor in hypertension, it has also been reported to play a central role in proliferation and/or differentiation in specific organs, linking it to the progression of cancer (13, 14). Previously, we have reported that angiotensin II facilitates the secretion of some growth factors and cytokines from prostate stromal cells, resulting in cell proliferation of prostate cancer (16). Given that angiotensin II induces oxidative stress in vascular cells, it is very interesting to speculate that angiotensin II may function as an inducer of oxidative stress implicated in carcinogenesis. In the present study, we examined whether angiotensin II has the potential to evoke oxidative stress in prostate cancer cells. The expression of SOD2, one of the mitochondrial antioxidant enzymes, was time-dependently enhanced by angiotensin II treatment in prostate cancer cells (data not shown). Also, angiotensin II induced the expression of p47phox, one of cytosolic NADPH oxidases, whereas the angiotensin receptor blocker candesartan (CV11974) inhibited its expression in prostate cancer cells. Furthermore, angiotensin II induced the expression of antioxidant enzymes, glutathione peroxidase, and SOD2, and candesartan inhibited their expression. It is well known that oxidative stress induces DNA and protein adducts, and similarly, angiotensin II induced the expression of 8-OHdG and modification of protein with 4-hydroxynonenal expression in prostate cancer cells.

Early reports revealed the existence of RAS in the prostate; all components of RAS, including angiotensinogen, renin, ACE, and angiotensin receptors (27-31), have been identified in the prostate. Intriguingly, a 3-fold to 5-fold higher concentration of angiotensin II was confirmed in seminal fluid in comparison with that in blood (32), which strongly supports the existence of RAS in the prostate gland. Likewise, it was reported that there was a high concentration of angiotensin II in pancreatic cancer tissue compared with that in normal tissue (33), and RAS components, including angiotensinogen, angiotensin II receptor type 1, and renin, have been identified in the islets of Langerhans (34). These findings provide supportive evidence that the local RAS in these organs, especially angiotensin II, may exert paracrine effects in the development of prostate and pancreatic cancer. The possible mechanism of carcinogenesis by angiotensin II is expected to be induction of oxidative stress in these organs.

We previously clarified that angiotensin II acted as a growth factor in prostate cancer and stromal cells (14, 16). Interestingly, earlier investigators have reported that angiotensin II induced oxidative stress in vascular cells, for example, demonstrating that angiotensin II stimulated the production of ROS in endothelial cells by up-regulating the subunits of NADPH oxidases (17, 18). In the present study, we confirmed that angiotensin II–induced production of the O_2^- radical in prostate cancer cells, as shown in Fig. 5. Higashi et al. confirmed that NADPH oxidase is the most important source of ROS in the vasculature (35). It is well known that NAPDH oxidase is composed of cytosolic components, such as p47phox, p67phox, and RC1, and membrane-spanning components, such as p22phox and gp91phox. Angiotensin II–induced NADPH oxidase activation is one of the major sources of ROS in the pathophysiologic mechanism of atherosclerosis (35, 36). These observations are consistent with the findings of the present study, in which angiotensin II induced the expression of p47phox and production of the O_2^- radical.

It is likely that induction of ROS subjects the cell to a state of oxidative stress, leading to damage of cellular DNA and proteins (37). A growing body of evidence has shown that excessive lipid peroxidation generated by oxidative stress may be involved in carcinogenesis. Especially, 4-hydroxynonenal is a major product of lipid peroxidation, and its level becomes relatively high in cells under oxidative stress (38). An augmented level of 4-hydroxynonenal was observed in oxidative stress-related degenerative diseases (39, 40). Furthermore, accumulation of 8-OHdG has been shown to lead to G:C-to-T:A transversion mutations that are prevalent in mutated oncogenes and tumor suppressor genes (41, 42). As shown in the present data, angiotensin II stimulation augmented DNA and protein markers, such as 8-OHdG, in prostate cancer cells. In general, DNA damage triggers the cell cycle checkpoints G_2-M and G_1-S through activation of kinases, e.g., phosphorylation of Chk2 at Thr^{68} and multiple sites in p53 (43, 44). Our data also showed that angiotensin II induced the phosphorylation of Chk2 (Tbr^{68}) and p53 (Ser^{15}). Chronic oxidative stress has been implicated in neoplastic transformation (45) and promotion of tumorigenesis (46). The present study provides evidence that ROS generated by angiotensin II may contribute to

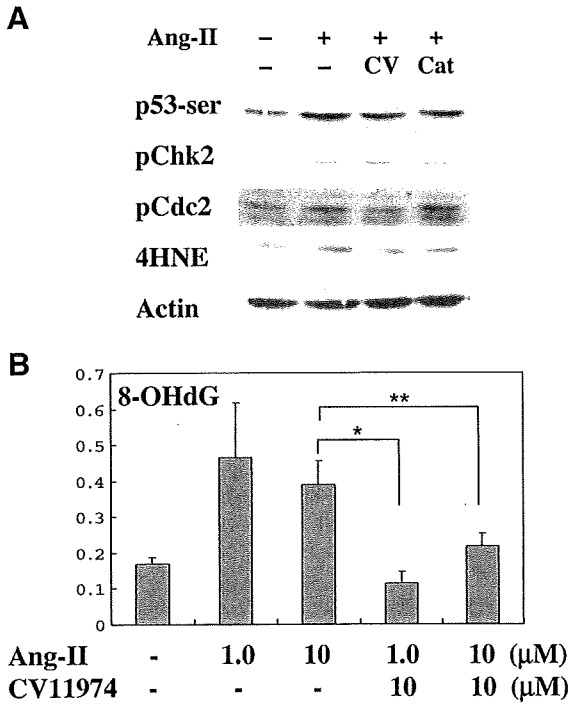

FIGURE 7. DNA damage in LNCaP cells by angiotensin II treatment. **A.** LNCaP cells were pretreated with 10 μmol/L candesartan or 1,000 units/mL catalase for 30 min and harvested after 24 h of 10 μmol/L angiotensin II exposure. Western blots of protein lysates (20 μg) were probed with antibodies to checkpoint proteins, including phosphorylated p53 (Ser^{15}), phosphorylated Chk2 (Thr^{68}), phosphorylated cdc2 (Tyr^{15}), and actin. To examine the DNA damage by angiotensin II treatment, Western blot was also done using anti–4-hydroxynonenal (*4HNE*) antibody. **B.** 8-OHdG level was measured after treatment with angiotensin II at the indicated concentrations or simultaneously with 10 μmol/L candesartan (CV11974). Columns, mean of three different experiments; bars, SD. Candesartan (CV11974) treatment significantly suppressed 8-OHdG level induced by 1 or 10 μmol/L CV11974 treatment (* or **, $P < 0.05$).

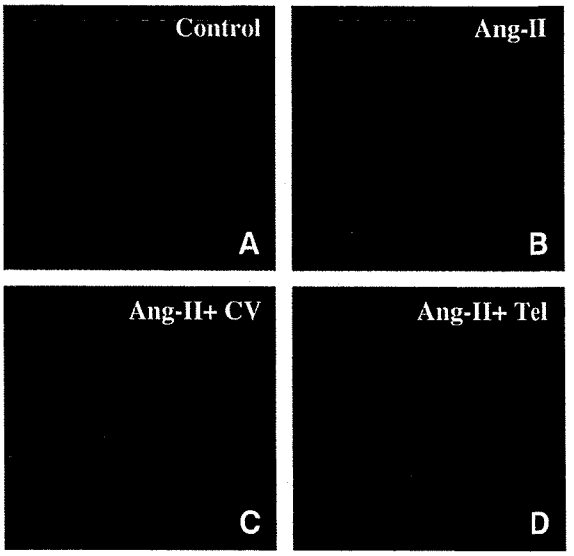

FIGURE 8. Immunocytochemical staining of iNOS in LNCaP cells. Intracellular expression of iNOS was induced by stimulation with 10 μmol/L angiotensin II (**B**) compared with the control (**A**), whereas 10 μmol/L CV11974 and 1 μmol/L telmisartan, an ARB, diminished iNOS expression induced by angiotensin II treatment (**C** and **D**).

DNA damage and be involved in carcinogenesis of the prostate gland.

The present data showing that angiotensin II enhanced iNOS expression and ARBs inhibited it in prostate cancer cells support the evidence that angiotensin II is a peptide involved in inflammation. In vascular smooth muscle cells, iNOS may be induced by various cytokines, including interleukin 1β, tumor necrosis factor α, IFN-γ, and interleukin 6 (47). Also, iNOS was strongly observed in inflamed epithelium. Earlier studies have shown that iNOS is expressed in epithelial cells in patients with colitis who are prone to colon cancer (48-50). Regarding the link between iNOS and cancer development, the expression of iNOS was higher in cancer specimens than in normal tissue in esophageal, colon, and thyroid carcinomas (51, 52). Baltaci et al. reported that the expression of iNOS was higher in high-grade PIN and prostatic carcinoma samples than in benign prostatic hypertrophy and low-grade PIN samples. These findings suggest that nitric oxide produced by iNOS may be involved in prostate tumorigenesis (53). In addition, Calvisi et al. revealed that iNOS and NADPH oxidase were involved in ROS generation during c-Myc/transforming growth factor α hepatocarcinogenesis and were inhibited by antioxidant agent treatment (54).

There have recently been several reports suggesting a relationship between chronic inflammation and prostate cancer. It is plausible that ROS released by inflammatory cells during cycles of cellular damage and regeneration in the organ result in permanent DNA damage (55). The prostate gland is a common site of chronic inflammation. Although most focal lesions of prostatic atrophy are considered quiescent, prostate epithelial cell proliferation is increased in some lesions, and thus, focal prostatic atrophy, which is associated with chronic inflammation, is considered to be proliferative (56).

Pathologic findings support the hypothesis that chronic inflammation may be involved in prostate cancer development. Novel observations have been reported regarding the pathologic entity of focal prostatic epithelial atrophy (57), which is associated with chronic inflammation with proliferative change, designated "proliferative inflammatory atrophy." More interestingly, these areas are commonly adjacent to high-grade PIN or local foci of cancer in the prostate of older men (58). Proliferative inflammatory atrophy lesions have been regarded as a precursor lesion of prostate cancer (59). In an experimental study, prostatic tissue with inflammation caused by bacterial infection showed atypical hyperplasia and areas of dysplasia showed stronger staining for oxidative DNA damage and greater epithelial cell proliferation than normal prostatic gland (60). The pathogenesis of the development of prostate cancer possibly involves ROS generated through various actions of androgen, infection, or angiotensin II, as mentioned above. Theoretically, it is proposed that long-term exposure to ROS may cause DNA and protein damage, cell proliferation, and enhancement of oncogenes, linking it to the development of proliferative inflammatory atrophy, PIN, and, finally, prostate cancer (Fig. 9).

Androgen is also likely to play a central role in prostate carcinogenesis. There has been increasing evidence to support the hypothesis that oxidative stress induced by androgen, at least in part, contributes to carcinogenesis. Androgen-induced ROS may directly or indirectly result from its influence on mitochondria (61). An *in vitro* study using androgen-sensitive human prostate cancer cells, LNCaP, showed that stimulation with a physiologic level of androgen resulted in an increased level of ROS (62). Supporting this hypothesis, Sun et al. suggested that prostate-specific antigen, a representative androgen-dependent protein, markedly stimulates the generation of ROS in LNCaP cells. They also showed that the effect of testosterone on ROS was suppressed by flutamide and by anti–prostate-specific antigen antibody (63).

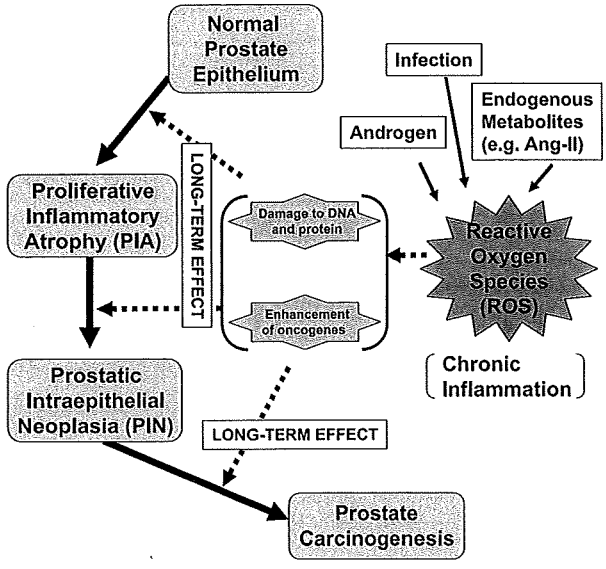

FIGURE 9. Pathogenesis of prostate cancer possibly involves ROS generated by various actions of androgen, infection, or angiotensin II. Theoretically, it is proposed that long-term exposure to ROS causes DNA and protein damage, cell proliferation, and enhancement of oncogenes, linking it to the formation of proliferative inflammatory atrophy (*PIA*), PIN, and, finally, prostate cancer.

In conclusion, epidemiologic, experimental, and clinical studies have implicated oxidative stress in the development and progression of prostate cancer. The present study indicated that oxidative stress caused by the local generation of angiotensin II may be involved in the development of prostate cancer. A greater understanding of the molecular events associated with oxidative stress will contribute to better strategies for the chemoprevention of prostate cancer.

Materials and Methods

Cell Lines

LNCaP cells, a human prostate cancer cell line, were obtained from the American Type Culture Collection. LNCaP cells were cultured in F-12 medium supplemented with 10% FCS under 5% CO_2 before the experiments. In the experiments, LNCaP cells were cultured in phenol red–free RPMI plus 0.1% bovine serum albumin and stimulated with reagents. Cells were used for each experiment within 10 to 12 passages.

Reagents

Angiotensin II was purchased from Auspep Pty. Anti-SOD2 antibody was purchased from Millipore. Anti-p47phox, anti-AT1 receptor, and anti-iNOS antibodies were purchased from Santa Cruz Biotechnology. Anti–4-hydroxynonenal antibody was purchased from NOF Co. Anti-Akt, phosphorylated Akt, phosphorylated p53 (Ser^{15}), phosphorylated Chk2 (Thr^{68}), and phosphorylated cdc2 (Tyr^{15}) antibodies were purchased from Cell Signaling Technology. Catalase, PEG-SOD, and LY294002 were purchased from Sigma. The ARBs candesartan (CV11974) and telmisartan were provided by Takeda Pharmaceutical Co. and Boehringer Ingelheim, respectively.

Immunocytochemical Staining

Cells plated on culture slides, Lab-Tek Chamber Slide (Nalge Nunc International), were rinsed with PBS twice before they were fixed in 2% paraformaldehyde/PBS at room temperature for 15 min. Fixed cells were washed with 100 mmol/L ammonium chloride for 10 min and permeabilized with 0.1% Triton X-100/PBS for 10 min. These cells were blocked with 10% normal goat serum/PBS for 1 h. Primary antibody against iNOS was diluted 1:100 in 10% normal goat serum/TBST [20 mmol/L Tris-HCl (pH 8.0), 150 mmol/L NaCl, 0.05% Tween 20] and applied for 1 h in a 37°C chamber. After an additional three washes with TBST for 5 min, cells were incubated with Cy3-labeled secondary antibody for 1 h in a 37°C chamber. Before cells were mounted in antifade reagent, they were washed thrice in TBST for 5 min. As a control, sections were incubated without treatment with angiotensin II or nonprimary antibody. Images were captured using a fluorescence microscope (BZ-8000; Keyence).

Superoxide Anion (O_2^-) Assay

Dihydroethidium (HE), which is a specific dye for O_2^-, is oxidized by O_2^- to ethidium, which stains the nucleus a bright